JCTC Journal of Chemical Theory and Computation

pubs.acs.org/JCTC Article

Reference CC3 Excitation Energies for Organic Chromophores: Benchmarking TD-DFT, BSE/*GW*, and Wave Function Methods

Iryna Knysh, Filippo Lipparini, Aymeric Blondel, Ivan Duchemin, Xavier Blase, Pierre-François Loos,* and Denis Jacquemin*

Cite This: *J. Chem. Theory Comput.* 2024, 20, 8152−8174 Read Online

ACCESS | Metrics & More | Article Recommendations | Supporting Information

ABSTRACT: To expand the QUEST database of highly accurate vertical transition energies, we consider a series of large organic chromogens ubiquitous in dye chemistry, such as anthraquinone, azobenzene, BODIPY, and naphthalimide. We compute, at the CC3 level of theory, the singlet and triplet vertical transition energies associated with the low-lying excited states. This leads to a collection of more than 120 new highly accurate excitation energies. For several singlet transitions, we have been able to determine CCSDT transition energies with a compact basis set, finding minimal deviations from the CC3 values for most states. Subsequently, we employ these reference values to benchmark a series of lower-order wave function approaches, including the popular ADC(2) and CC2 schemes, as well as time-dependent density-functional theory (TD-DFT), both with and without applying the Tamm−Dancoff approximation (TDA). At the TD-DFT level, we evaluate a large panel of global, range-separated, local, and double hybrid functionals. Additionally, we assess the performance of the Bethe−Salpeter equation (BSE) formalism relying on both G_0W_0 and ev*GW* quasiparticle energies evaluated from various starting points. It turns out that CC2 and ADC(2.5) are the most accurate models among those with respective $O(N^5)$ and $O(N^6)$ scalings with system size. In contrast, CCSD does not outperform CC2. The best performing exchange−correlation functionals include BMK, M06−2X, M06-SX, CAM-B3LYP, ωB97X-D, and LH20t, with average deviations of approximately 0.20 eV or slightly below. Errors on vertical excitation energies can be further reduced by considering double hybrids. Both SOS-ωB88PP86 and SOS-ωPBEPP86 exhibit particularly attractive performances with overall quality on par with CC2, whereas PBE0-DH and PBE-QIDH are only slightly less efficient. BSE/ev*GW* calculations based on Kohn−Sham starting points have been found to be particularly effective for singlet transitions, but much less for their triplet counterparts.

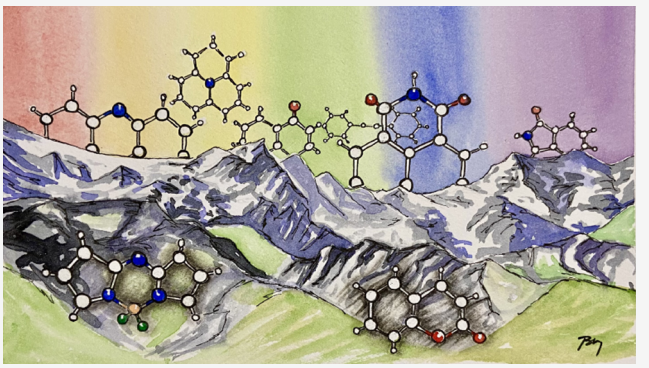

1. INTRODUCTION

Organic dyes are everywhere, permeating countless aspects of our daily lives and playing pivotal roles in numerous applications. From the hues enhancing clothing and textiles to the intricate colors illuminating our electronic displays, organic dyes are indispensable to fashion, energy conversion, imagining, sensing, etc. However, accurately simulating the colors produced by dyes and pigments poses a persistent challenge for theoretical chemists, largely owing to the remarkable sensitivity of the human eye, albeit confined to a limited region of the electromagnetic spectrum. Indeed, in the blue-green region, humans can distinguish color differences corresponding to changes in the absorption wavelength as tiny as 0.5−1.0 nm (approximately 0.005 eV). Achieving this level of accuracy is currently beyond the capabilities of quantum many-body methods for molecules that absorb visible light.

Despite this challenge, the quantum chemical modeling of absorption properties of organic dyes has been steadily advancing. A notable early contribution came from Adachi and Nakamura, who employed semiempirical methods (CNDO/S and INDO/S) to investigate the excited-state (ES) properties of approximately 30 real-life dyes, drawn from popular chromophore families like azobenzene, anthraquinone, and hydrazone.[1] In this work of 1991, the vertical transition energies (VTEs) were directly compared with the experimental wavelengths of maximal absorption (λ_{max}) and the computed oscillator strengths (f) were correlated with the measured molar absorptivity coefficients ($\log \epsilon$), an approach that remains popular despite its intrinsic shortcomings.[2] Notably, the INDO/S method emerged as the most satisfactory,

Received: July 12, 2024
Revised: August 20, 2024
Accepted: August 27, 2024
Published: September 5, 2024

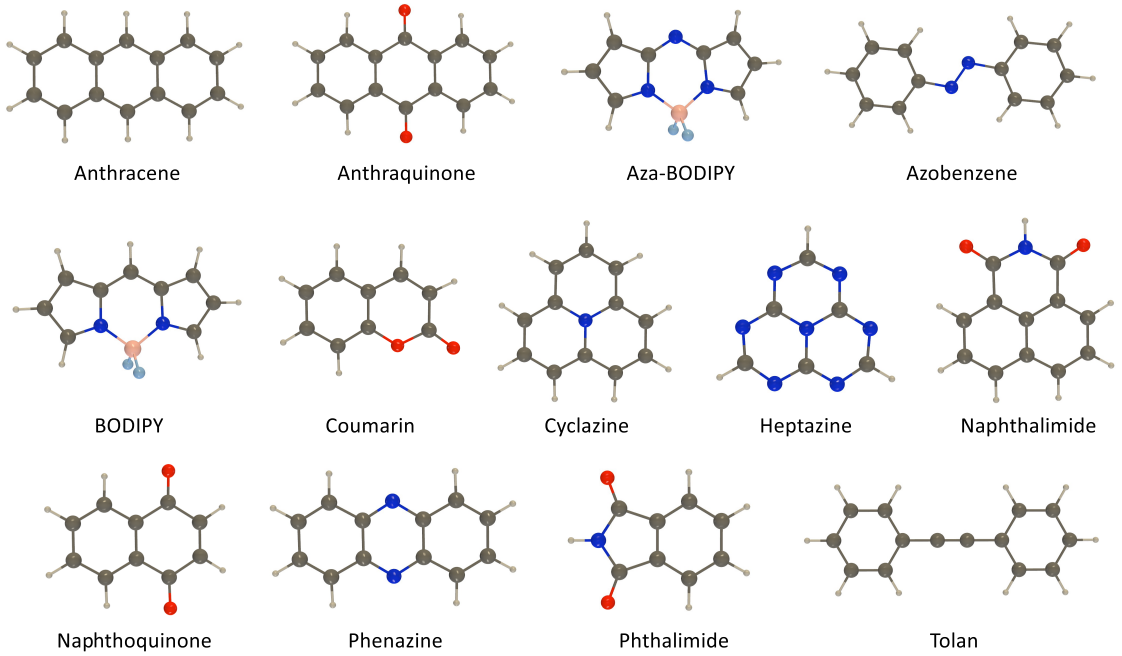

Figure 1. Representation of the systems investigated in the present study.

yielding a mean absolute error (MAE) of 0.48 eV and a linear correlation coefficient R = 0.60 when compared to experimental data. Clearly, these values fall short of enabling precise color prediction or the design of new dyes.

A decade later, the same group proposed an analogous investigation for a similar set of transitions but relying on time-dependent density-functional theory (TD-DFT)[3,4] using two exchange−correlation functionals (XCFs): BPW91 and B3LYP.[5] With the B3LYP global hybrid (GH), they reached a MAE of 0.19 eV, which they deemed "quite satisfactory". Later on, one of us applied TD-DFT on much larger and more diverse sets of organic dyes using an extended panel of XCFs.[6,7] However, even with the most effective hybrid functional tested at that time, PBE0, the MAE obtained remained similar at 0.22 eV.

Two primary factors contribute to the magnitude of these errors. First, the aforementioned works fail to consider vibronic couplings, which are crucial for achieving robust comparisons between experimental observations and theoretical predictions.[8−12] Indeed, as demonstrated by Dierksen and Grimme two decades ago for a set of 43 transitions in π-conjugated organic derivatives, including vibronic couplings allows for more meaningful comparisons between theory and experiment as band shapes are obtained. Nevertheless, the MAE on 0−0 energies remained essentially unchanged (0.18 eV with the BH&HLYP functional).[8] Second, despite the elegance and potency of adiabatic TD-DFT, its inherent approximations do not allow to systematically achieve a high level of accuracy, particularly when relying on a single XCF, since ESs of various natures ideally require different XCFs. For example, GHs are more suitable for valence transitions while charge-transfer (CT) excitations usually require range-separated hybrids (RSHs).[13]

On the theoretical side, several methods are available to get more accurate VTEs.[14] First, one can further climb Jacob's ladder of DFT, opting for double hybrids (DHs) rather than GHs or RSHs.[15−18] Second, another approach involves employing the Bethe−Salpeter equation (BSE) formalism[19,20] of many-body perturbation theory[21,22] combined with the *GW* method.[23−26] The so-called BSE/*GW* approach advantageously washes out the XCF dependency, when a (partially) self-consistent *GW* scheme is used.[27−29] The diagonalization of the electron−hole BSE Hamiltonian in the (de)excitation space offers the same computational scaling as Casida's formulation of TD-DFT,[3] namely $O(N^4)$ to get iteratively the lowest eigenvalues. Similarly, the preceding *GW* calculations, required to obtain the quasiparticle energies and screened Coulomb potential that enter the BSE Hamiltonian, can be performed with $O(N^4)$ scaling using resolution-of-the-identity (RI) techniques. Third, one can opt for correlated wave function approaches. Within this framework, the systematically improvable coupled-cluster (CC) route stands as a natural choice, offering a clear path for increases in accuracy with its CC2,[30,31] CCSD,[32−36] CC3,[37−39] CCSDT,[40−44] CC4,[45−48] CCSDTQ,[45,49−51] and so forth declinations.

This is the approach we primarily employed to build the QUEST database,[52] which currently includes over 500 VTEs considered chemically accurate, that is, with a deviation below 0.05 eV from the exact result. QUEST relies on diffuse containing basis sets, and most results are, at least, of aug-cc-pVTZ quality. While this 0.05 eV value falls short of the human eye's ability in terms of accuracy, these reference VTEs are nonetheless useful for both methodological benchmarking purposes[52] and for comparisons of various chemical strategies aiming at tailoring ES energies. In the initial release of the QUEST database,[52] the largest compounds considered were naphthalene and one of its tetra-aza analogues. These two highly symmetric bicyclic compounds contain 10 heavy (non-H) atoms. In 2021, we expanded this data set by incorporating other, less symmetric bicyclic compounds, including real-life chromophores like diketopyrrolopyrrole, yet none larger than 10 non-H atoms.[53] A key finding from this 2021 work is the notable differences in the relative accuracies of the benchmarked wave function methods compared to those

https://doi.org/10.1021/acs.jctc.4c00906
J. Chem. Theory Comput. 2024, 20, 8152−8174

observed for smaller molecules. For instance, while CCSD provides very accurate VTE estimates for small molecules, its precision clearly diminishes for larger compounds.[52,53]

The present contribution aims at providing accurate VTEs for the series of real-life chromogens represented in Figure 1. We clearly draw inspiration from previous studies,[1,5,7,54] with a focus on the most important classes of organic chromophores and fluorophores.[55−57] Naturally, for molecules of such size, incorporating quadruple excitations at the CC level, as recently accomplished for five and six-membered rings,[48] or sufficiently converging selected configuration interaction calculations[58−60] is simply beyond reach.[61−63] However, obtaining CC3 values in a reasonably large basis set remains feasible. Moreover, it is even sometimes possible to perform CCSDT calculations, albeit in a relatively compact basis set.

To the best of our knowledge, these are the first high-level calculations reported for a large panel of chromophores. In fact, we are not aware of any previous CC3 calculation published for any of the compounds of Figure 1, except for CC3/aug-cc-pVDZ values obtained for azobenzene,[64,65] and our recent contribution on the lowest singlet and triplet ESs of cyclazine and heptazine computed at the CC3/aug-cc-pVTZ level.[66]

There are nevertheless a few CC3 literature precedents that deserve to be highlighted, the first of which is the seminal series of works from Thiel and co-workers who obtained an impressive list of CC3/TZVP VTEs for organic compounds (the largest system being naphthalene).[67,68] There are also more specific works using CC3 on rather large molecules. For example, Zuev et al. investigated two isomers of *p*-coumaric acid (12 non-H atoms) at the CC3/6−31+G(d,p) level,[69] Kánnár and Szalay studied numerous ESs of the DNA bases (largest one being composed of 10 non-H atoms) at CC3/TZVP level,[70] Hutcheson and co-workers modeled the two lowest ESs of azobenzene (14 non-H atoms) at the CC3/aug-cc-pVDZ level, Cuzzocrea et al. used CC3/aug-cc-pVDZ to tackle increasingly long cyanine chains up to 15 non-H atoms,[71] Gui and co-workers obtained CC3/TZVP estimates for a series of push−pull systems (up to 11 non-H atoms),[28] and we obtained CC3/cc-pVTZ values for 28 CT ESs (as large as 12 non-H atoms).[72] In these two latter cases, further basis set corrections were applied to account for the lack of diffuse basis functions.

Even larger systems can be considered if one relies on local correlation methods. Notably, Hättig's group performed a CC3/aug-cc-pVTZ calculation of the lowest ES of berenil (29 non-H atoms) using their pair-natural-orbital implementation,[73] whereas Koch's group determined multilevel/natural-transition-orbital CC3/aug-cc-pVDZ valence VTEs on azobenzene (14 non-H atoms),[65,74] and the core excitations of betaine30 (43 non-H atoms). At the CCSD level of theory, the number of studies is too large to be listed. Yet, we wish to highlight the 2019 work of Martinez's group.[54] Using a rank-reduced version of CCSD, they tackled 19 ESs in 8 real-life dyes.[54] This represents the closest attempt at using high-level CC methods for estimating VTEs in large dyes we are aware of. In addition, many works rely on CC2 or its algebraic diagrammatic construction counterpart, ADC(2), for estimating VTEs in photoactive systems (see, for example, refs 75−79).

This paper is organized as follows. In Section 2, we detail the protocols used to perform our calculations. In Section 3, we first present the obtained reference values and comment on their nature and accuracy. We then provide comparisons with selected literature data. Next, we turn to the benchmark of wave function-based, density-based, and one-body Green's function-based approaches before closing the result section with further discussion about the change of reference values and a specific challenging case. Section 4 summarizes our main findings.

2. COMPUTATIONAL DETAILS

2.1. Generalities. All calculations presented in this study are conducted, except when noted, under the frozen-core approximation and typically use the default convergence thresholds of the chosen electronic structure softwares. We underline that distinct symmetry conventions concerning molecular orientations in various codes may lead to distinct state labeling for molecules belonging to the C_{2v} ($B_1 \leftrightarrow B_2$) and D_{2h} ($B_{1x} \leftrightarrow B_{2x} \leftrightarrow B_{3x}$, with $x = g$ or u) point groups. To address this potential difficulty, we provide in the Supporting Information (SI) various information regarding each state (see below) enabling quick identification of the ESs of interest. It is worth mentioning that, in the subsequent discussion, we do not specify the equation-of-motion (EOM) or linear-response (LR) prefixes for the CC methods, as both formalisms yield identical VTEs. The CCSD/aug-cc-pVTZ oscillator strengths listed in the SI have been determined with LR-CCSD.

2.2. Geometries. The ground-state structures of all compounds were optimized at the CCSD(T)/cc-pVTZ level using CFOUR 2.1,[80,81] building *Z*-matrices to enforce the relevant point group symmetry. For both aza-BODIPY and BODIPY, the C_{2v} point group was selected for obvious computational reasons, though the fluoroborate moiety should normally be slightly out-of-plane leading to C_s ground-state structures. The optimal structures of all compounds are shown in Figure 1 and Cartesian coordinates are provided in the SI.

2.3. Reference Excitation Energies. For a given molecule, we typically start our exploration by performing a CCSD/aug-cc-pVTZ calculation for 8−12 singlet and triplet ESs using GAUSSIAN16,[82] so as to identify a series of relevant low-lying ESs. We next perform CC calculations for the targeted ESs with three basis sets, namely, 6−31+G(d), aug-cc-pVDZ, and aug-cc-pVTZ, which are dubbed as "Pop", "AVDZ", and "AVTZ" in the following. We underline that the selection of these three bases is motivated by their incorporation of both polarization and diffuse functions, in addition to their widespread availability. In particular, AVTZ is commonly acknowledged to yield valence excitation energies close to the complete basis set limit and provides reasonable VTE estimates for most Rydberg's ESs. Besides GAUSSIAN, CCSD and CC3 calculations are performed with CFOUR and DALTON,[83] the latter advantageously allowing CC3 triplet ES calculations. All CCSDT results presented here have been obtained with CFOUR. In CFOUR, converging the self-consistent field (SCF) procedure typically required a quadratic SCF algorithm together with fixed occupation numbers for each symmetry. In a few cases, we had to ramp up to 10^{-6} the linear dependency threshold to converge the SCF and CC calculations. Likewise, the default number of expansion vectors in the iterative CC subspace had to be increased to reach convergence of the CC ground-state amplitudes in some cases. For several ESs, we compared the CCSD/aug-cc-pVTZ VTEs obtained with the three codes and did not observe any difference larger than 0.010 eV (a discrepancy obtained for a

https://doi.org/10.1021/acs.jctc.4c00906
J. Chem. Theory Comput. 2024, 20, 8152−8174

Rydberg transition in anthracene) with the vast majority of VTEs agreeing to 0.001 eV.

To produce the theoretical best estimate (TBE) associated with each VTE, $\Delta E^{\mathrm{TBE}}_{\mathrm{AVTZ}}$, we typically select the CC3/AVTZ value when available, that is

$$\Delta E^{\mathrm{TBE}}_{\mathrm{AVTZ}} = \Delta E^{\mathrm{CC3}}_{\mathrm{AVTZ}} \quad (1)$$

When we could afford to compute the CCSDT/Pop value, $\Delta E^{\mathrm{CCSDT}}_{\mathrm{Pop}}$, we relied on the following expression instead

$$\Delta E^{\mathrm{TBE}}_{\mathrm{AVTZ}} = \Delta E^{\mathrm{CC3}}_{\mathrm{AVTZ}} + [\Delta E^{\mathrm{CCSDT}}_{\mathrm{Pop}} - \Delta E^{\mathrm{CC3}}_{\mathrm{Pop}}] \quad (2)$$

which has been shown to provide a reasonable estimate of the true $\Delta E^{\mathrm{CCSDT}}_{\mathrm{AVTZ}}$ value.[48] In contrast, when CC3/AVTZ is beyond reach, which is typically the case for triplet ESs, we relied on the two following equations

$$\Delta E^{\mathrm{TBE}}_{\mathrm{AVTZ}} = \Delta E^{\mathrm{CCSDR(3)}}_{\mathrm{AVTZ}} + [\Delta E^{\mathrm{CC3}}_{\mathrm{AVDZ}} - \Delta E^{\mathrm{CCSDR(3)}}_{\mathrm{AVDZ}}] \quad (3)$$

$$\Delta E^{\mathrm{TBE}}_{\mathrm{AVTZ}} = \Delta E^{\mathrm{CCSD}}_{\mathrm{AVTZ}} + [\Delta E^{\mathrm{CC3}}_{\mathrm{AVDZ}} - \Delta E^{\mathrm{CCSD}}_{\mathrm{AVDZ}}] \quad (4)$$

to approach the true $\Delta E^{\mathrm{CC3}}_{\mathrm{AVTZ}}$ value, for singlets and triplets respectively. This composite procedure is quite popular in the CC community.[28,45,68,72,84−91] Indeed, it is common to correct double-ζ values obtained with a high excitation degree with triple-ζ estimates determined at a lower excitation level. We refer the interested reader to ref 48. for exhaustive tests of this approach in a similar context.

In Tables S1−S4 of the SI, we provide, for all considered ESs, the raw VTEs computed at the CCSD, CCSDR(3), CC3, and CCSDT levels of theory with the three above-mentioned basis sets, together with several additional characteristics: (i) the percentage of single excitations, $\%T_1$, as given at the CC3/AVDZ level by DALTON; (ii) the LR-CCSD/AVTZ oscillator strengths, f, provided by GAUSSIAN; (iii) the spatial extend of the ES (and ground state), $\langle r^2 \rangle$, determined at the ADC(2)/AVTZ level with Q-CHEM 6.0 (see below for details);[92] and (iv) the dominant Hartree−Fock (HF) molecular orbital contributions for each CCSD/AVTZ transition as computed with GAUSSIAN.

2.4. Benchmarks. The TBEs described above have been used to assess a series of popular wave function, density, and one-body Green's function methods. All these benchmark calculations were performed with the AVTZ basis set. Using the criteria detailed above, identifying the various ES across the benchmarked methods was generally tedious yet straightforward. All results are listed in the SI for each method detailed below.

2.4.1. Wave Function Calculations. We have used TURBOMOLE (7.3/7.5/7.8)[93,94] to determine the VTEs for 5 second-order methods, namely, CIS(D),[95,96] CC2,[30,31] SOS-ADC(2), SOS-CC2, and SCS-CC2.[97] In these calculations, the RI approximation was systematically enforced, and default SOS and SCS parameters were applied. We have chosen Q-CHEM[92] to perform the EOM-MP2,[98] ADC(2),[99,100] SOS-ADC(2),[101] and, when computationally feasible, ADC(3)[100,102,103] calculations. These methods also take advantage of the RI implementation whereas the electron repulsion integral accuracy threshold was tightened to 10^{-14}. Q-CHEM and TURBOMOLE use different SOS parameters. Therefore, two nonequivalent SOS-ADC(2) methods have been benchmarked. These are distinguished by the additional labels, [QC] and [TM], for Q-CHEM and TURBOMOLE, respectively. Within the composite ADC(2.5) approach proposed by some of us,[104] VTEs were simply determined as the average of the ADC(2) and ADC(3) results. We note that this simple half and half ratio was later shown to be nearly optimal by Dreuw's group.[105] As explained above, GAUSSIAN16[82] was used for the CCSD calculations.[32] DALTON[83] was selected to computed the CCSDR(3) transition energies,[106] whereas CFOUR was employed to compute both the CCSD(T)(a)*[107107] and CCSDT-3[108,109] energies.

2.4.2. TD-DFT Calculations. GAUSSIAN16 was employed to perform the TD-DFT calculations using GHs and RSHs, except for a few cases where we relied on TURBOMOLE ([TM]) or Q-CHEM ([QC]) instead (see below). We did not select any "pure" functionals, such as BLYP or PBE, as they are well-known to provide, compared to hybrids, less accurate VTEs for organic compounds.[13] The following 11 GHs were considered: TPSSh,[110] τ-HCTCH-hyb,[111] B3LYP,[112−115] PBE0,[116,117] SCAN0 [TM],[118] M06,[119] SOGGA11-X,[120] BMK,[121] MN15,[122] M08-HX,[123] and M06−2X.[119] We also considered 11 RSHs, namely, M06-SX [TM],[124] CAM-B3LYP,[125] tCAM-B3LYP [TM],[126] mCAM-B3LYP [TM],[127] rCAM-B3LYP [TM],[128] ωB97X-D,[129] ωB97M-V [QC],[130] ωB97X,[131] ωB97,[131] LC-ωHPBE,[132] and M11.[133] GAUSSIAN16 calculations use default parameters except for a tighter SCF convergence threshold (10^{-10}), TURBOMOLE calculations took advantage of the RI (and when possible RI-JK) approaches and we set a 10^{-9} SCF convergence threshold and a large quadrature grid (*gridsize* = 7), whereas Q-CHEM calculations were done without RI approximation and with tighten convergence parameters.[134]

It is important to note that VTEs obtained with meta-GGA-based hybrids are known to be gauge-dependent.[135,136] This effect is not accounted for in GAUSSIAN, although Q-CHEM and TURBOMOLE propose a gauge invariance correction, the latter code computing it by default. Previous works have assessed the importance of this correction for small molecules,[136−138] as well as for ES properties of larger compounds.[138] To evaluate the impact of the gauge invariance on VTEs, we have performed additional M06, M06−2X, and M06-SX calculations with TURBOMOLE (in addition to GAUSSIAN for the two former). To distinguish between these two sets of results, an additional prefix "c" is added to the name of the XCF. For example, cM06−2X corresponds to the gauge-corrected version of M06−2X.

ORCA 5.0[139] was selected to perform the DH calculations using the *tightSCF* and *grid3* options and applying the RI with the automatically generated auxiliary basis set. The following 9 DHs were tested: B2PLYP,[140] PBE0-DH,[141] PBE-QIDH,[142] ωB2PLYP,[90] RSX-0DH,[143] RSX-QIDH,[144] ωB97X-2,[145] SOS-ωB88PP86,[146] and SOS-ωPBEPP86.[146]

Finally, TURBOMOLE 7.8 was used for the local hybrid (LH) calculations. We used the same parameters as given above, including the large grid (*gridsize* = 7) and considered 3 functionals, namely, LH12ct-SsirPW92,[147] LH14t-calPBE,[148] and LH20t.[149] The above-mentioned gauge corrections were applied. Hence, all these XCFs are denoted with the "c" prefix in the following.

For all XCFs, we performed two sets of calculations, one using the "full" TD-DFT approach and one using the Tamm−Dancoff approximation (TDA). The only exception was the triplet ESs obtained with DHs that were determined with the TDA only. In case of triplet instabilities,[150−152] some codes, e.g., TURBOMOLE, simply stop the calculations whereas others go on (such as GAUSSIAN) and eventually print negative VTEs, while some try to alleviate the problem by removing the

https://doi.org/10.1021/acs.jctc.4c00906
J. Chem. Theory Comput. 2024, 20, 8152−8174

Table 1. Theoretical Best Estimates of the VTEs (in eV) for All Considered ESs and the Corresponding Equation Selected to Define Each of Them

compound	state	TBE	method	compound	state	TBE	method
anthracene	$^1B_{1u}$ ($\pi \rightarrow \pi^*$)	3.757	eq 1		$^3A_1''$ (Ryd)	3.169	eq 4
	$^1B_{2u}$ ($\pi \rightarrow \pi^*$)	3.782	eq 1		$^3E''$ (Ryd)	3.693	eq 4
	$^1B_{3g}$ ($\pi \rightarrow \pi^*$)	5.012	eq 1	heptazine	$^1A_2'$ ($\pi \rightarrow \pi^*$)	2.717	eq 2
	$^1B_{2g}$ (Ryd)	5.078	eq 3		$^1A_1''$ ($n \rightarrow \pi^*$)	3.999	eq 2
	$^1B_{1u}$ ($\pi \rightarrow \pi^*$)	5.284	eq 1		$^1E''$ ($n \rightarrow \pi^*$)	4.108	eq 2
	$^1B_{3g}$ ($\pi \rightarrow \pi^*$)	5.291	eq 1		$^1E'$ ($\pi \rightarrow \pi^*$)	4.478	eq 2
	^1A_g ($\pi \rightarrow \pi^*$)	5.319	eq 1		$^3A_2'$ ($\pi \rightarrow \pi^*$)	2.936	eq 3
	$^1B_{3u}$ (Ryd)	5.379	eq 3		$^3E''$ ($\pi \rightarrow \pi^*$)	3.649	eq 3
	^1A_u (Ryd)	5.451	eq 3		$^3A_1''$ ($n \rightarrow \pi^*$)	3.992	eq 3
	$^1B_{2u}$ ($\pi \rightarrow \pi^*$)	5.476	eq 1		$^3E''$ ($n \rightarrow \pi^*$)	4.080	eq 3
	$^3B_{1u}$ ($\pi \rightarrow \pi^*$)	2.287	eq 4	naphthalimide	$^1B_2$ ($\pi \rightarrow \pi^*$)	4.033	eq 1
	$^3B_{3g}$ ($\pi \rightarrow \pi^*$)	3.655	eq 4		$^1B_1$ ($n \rightarrow \pi^*$)	4.145	eq 1
	$^3B_{2u}$ ($\pi \rightarrow \pi^*$)	3.708	eq 4		$^1A_1$ ($\pi \rightarrow \pi^*$)	4.155	eq 1
anthraquinone	$^1B_{1g}$ ($n \rightarrow \pi^*$)	3.226	eq 3		$^1A_2$ ($n \rightarrow \pi^*$)	4.632	eq 1
	^1A_u ($n \rightarrow \pi^*$)	3.466	eq 3		$^3A_1$ ($\pi \rightarrow \pi^*$)	2.780	eq 4
	^1A_g ($\pi \rightarrow \pi^*$)	4.104	eq 3		$^3B_2$ ($\pi \rightarrow \pi^*$)	3.785	eq 4
	$^1B_{2u}$ ($\pi \rightarrow \pi^*$)	4.219	eq 3		$^3B_1$ ($n \rightarrow \pi^*$)	4.060	eq 4
	$^1B_{3g}$ ($\pi \rightarrow \pi^*$)	4.321	eq 3		$^3B_2$ ($\pi \rightarrow \pi^*$)	4.124	eq 4
	$^1B_{1u}$ ($\pi \rightarrow \pi^*$)	5.101	eq 3		$^3A_2$ ($n \rightarrow \pi^*$)	4.519	eq 4
	$^1B_{2u}$ ($\pi \rightarrow \pi^*$)	5.406	eq 3	naphthoquinone	$^1B_1$ ($n \rightarrow \pi^*$)	3.023	eq 2
	$^3B_{1g}$ ($n \rightarrow \pi^*$)	3.010	eq 4		$^1A_2$ ($n \rightarrow \pi^*$)	3.215	eq 2
	^3A_u ($n \rightarrow \pi^*$)	3.262	eq 4		$^1A_1$ ($\pi \rightarrow \pi^*$)	4.115	eq 2
	$^3B_{1u}$ ($\pi \rightarrow \pi^*$)	3.443	eq 4		$^1B_2$ ($\pi \rightarrow \pi^*$)	4.342	eq 2
	$^3B_{3g}$ ($\pi \rightarrow \pi^*$)	3.498	eq 4		$^1A_2$ ($n \rightarrow \pi^*$)	5.436	eq 2
	^3A_g ($\pi \rightarrow \pi^*$)	3.740	eq 4		$^1A_1$ ($\pi \rightarrow \pi^*$)	5.458	eq 2
aza-BODIPY	$^1B_2$ ($\pi \rightarrow \pi^*$)	2.512	eq 2		$^1B_2$ ($\pi \rightarrow \pi^*$)	5.548	eq 2
	$^1B_2$ ($\pi \rightarrow \pi^*$)	3.457	eq 2		$^3B_1$ ($n \rightarrow \pi^*$)	2.796	eq 4
	$^1A_1$ ($\pi \rightarrow \pi^*$)	3.463	eq 2		$^3A_2$ ($n \rightarrow \pi^*$)	3.009	eq 4
	$^1B_1$ ($n \rightarrow \pi^*$)	3.881	eq 2		$^3B_2$ ($\pi \rightarrow \pi^*$)	3.316	eq 4
	$^3B_2$ ($\pi \rightarrow \pi^*$)	1.329	eq 4		$^3B_2$ ($\pi \rightarrow \pi^*$)	3.445	eq 4
	$^3B_2$ ($\pi \rightarrow \pi^*$)	2.774	eq 4		$^3A_1$ ($\pi \rightarrow \pi^*$)	3.760	eq 4
	$^3A_1$ ($\pi \rightarrow \pi^*$)	3.027	eq 4	phenazine	$^1B_{1u}$ ($n \rightarrow \pi^*$)	3.374	eq 1
	$^3B_1$ ($n \rightarrow \pi^*$)	3.435	eq 4		$^1B_{3u}$ ($\pi \rightarrow \pi^*$)	3.717	eq 1
azobenzene	^1B_g ($n \rightarrow \pi^*$)	2.871	eq 1		$^1B_{2u}$ ($\pi \rightarrow \pi^*$)	3.744	eq 1
	^1B_u ($\pi \rightarrow \pi^*$)	4.231	eq 1		$^1B_{1g}$ ($\pi \rightarrow \pi^*$)	4.497	eq 1
	^1A_g ($\pi \rightarrow \pi^*$)	4.439	eq 1		$^1B_{2g}$ ($n \rightarrow \pi^*$)	4.837	eq 1
	^1B_u ($\pi \rightarrow \pi^*$)	4.446	eq 1		^1A_u ($\pi \rightarrow \pi^*$)	5.115	eq 1
	^1A_g ($\pi \rightarrow \pi^*$)	5.185	eq 1		$^3B_{3u}$ ($\pi \rightarrow \pi^*$)	2.408	eq 4
	^3B_g ($n \rightarrow \pi^*$)	2.286	eq 4		$^3B_{1u}$ ($n \rightarrow \pi^*$)	3.055	eq 4
	^3B_u ($\pi \rightarrow \pi^*$)	2.800	eq 4		$^3B_{2u}$ ($\pi \rightarrow \pi^*$)	3.376	eq 4
	^3A_g ($\pi \rightarrow \pi^*$)	3.921	eq 4		$^3B_{1g}$ ($\pi \rightarrow \pi^*$)	3.554	eq 4
	^3B_u ($\pi \rightarrow \pi^*$)	4.218	eq 4	phthalimide	$^1B_1$ ($n \rightarrow \pi^*$)	4.186	eq 2
	^3A_g ($\pi \rightarrow \pi^*$)	4.279	eq 4		$^1A_1$ ($\pi \rightarrow \pi^*$)	4.600	eq 2
BODIPY	$^1B_2$ ($\pi \rightarrow \pi^*$)	2.771	eq 2		$^1A_2$ ($n \rightarrow \pi^*$)	4.795	eq 2
	$^1B_2$ ($\pi \rightarrow \pi^*$)	3.804	eq 2		$^1B_2$ ($\pi \rightarrow \pi^*$)	4.942	eq 2
	$^1A_1$ ($\pi \rightarrow \pi^*$)	3.901	eq 2		$^1B_2$ ($\pi \rightarrow \pi^*$)	5.921	eq 2
	$^3B_2$ ($\pi \rightarrow \pi^*$)	1.862	eq 4		$^1A_2$ ($n \rightarrow \pi^*$)	5.999	eq 2
	$^3B_2$ ($\pi \rightarrow \pi^*$)	3.110	eq 4		$^1A_1$ ($\pi \rightarrow \pi^*$)	6.306	eq 2
	$^3A_1$ ($\pi \rightarrow \pi^*$)	3.339	eq 4		$^3B_2$ ($\pi \rightarrow \pi^*$)	3.762	eq 1
coumarin	$^1A'$ ($\pi \rightarrow \pi^*$)	4.307	eq 1		$^3B_1$ ($n \rightarrow \pi^*$)	3.957	eq 1
	$^1A''$ ($n \rightarrow \pi^*$)	4.796	eq 1		$^3A_1$ ($\pi \rightarrow \pi^*$)	4.344	eq 1
	$^1A'$ ($\pi \rightarrow \pi^*$)	4.980	eq 1		$^3B_2$ ($\pi \rightarrow \pi^*$)	4.506	eq 4
	$^3A'$ ($\pi \rightarrow \pi^*$)	3.264	eq 4		$^3A_2$ ($n \rightarrow \pi^*$)	4.578	eq 1
	$^3A'$ ($\pi \rightarrow \pi^*$)	4.109	eq 4		$^3B_2$ ($\pi \rightarrow \pi^*$)	4.666	eq 4
	$^3A''$ ($n \rightarrow \pi^*$)	4.655	eq 4	tolan	$^1B_{2u}$ ($\pi \rightarrow \pi^*$)	4.724	eq 3
cyclazine	$^1A_2'$ ($\pi \rightarrow \pi^*$)	0.979	eq 2		$^1B_{3g}$ ($\pi \rightarrow \pi^*$)	4.746	eq 3

https://doi.org/10.1021/acs.jctc.4c00906
J. Chem. Theory Comput. 2024, 20, 8152−8174

Table 1. continued

compound	state	TBE	method	compound	state	TBE	method
	$^1E'$ ($\pi \rightarrow \pi^*$)	3.018	eq 2		$^1B_{1u}$ ($\pi \rightarrow \pi^*$)	4.796	eq 3
	$^1A_1''$ (Ryd)	3.163	eq 2		^1A_u ($\pi \rightarrow \pi^*$)	5.546	eq 3
	$^1E''$ (Ryd)	3.691	eq 2		$^1B_{3u}$ (Ryd)	5.598	eq 3
	$^3A_2'$ ($\pi \rightarrow \pi^*$)	1.110	eq 4		$^3B_{1u}$ ($\pi \rightarrow \pi^*$)	3.261	eq 4
	$^3E'$ ($\pi \rightarrow \pi^*$)	2.154	eq 4		^3A_g ($\pi \rightarrow \pi^*$)	4.061	eq 4

vectors associated with the problematic states as, for example, ORCA. Because of these distinct behaviors, we have thus chosen to remove all occurrences of triplet instabilities.

2.4.3. BSE/GW. Full and TDA-based BSE calculations have been performed starting from both nonself-consistent G_0W_0 and eigenvalue-self-consistent evGW procedures. Comparisons of evGW with various alternative GW procedures can be found elsewhere.[153,154] At the GW level, we corrected all occupied (i.e., frozen core approximation is not applied here) and 50 virtual orbitals for each molecule, higher levels being rigidly shifted following the highest explicitly corrected level. These calculations have been conducted using BEDEFT (beyond DFT).[155,156] The Coulomb-fitting RI (RI-V) techniques[157] and a robust analytic continuation scheme[156] have been employed during these calculations. The initial Kohn−Sham (KS) DFT (PBE0 and CAM-B3LYP) and HF calculations generating the starting eigenstates were performed with ORCA.[139]

3. RESULTS AND DISCUSSION

3.1. Theoretical Best Estimates. Our TBEs are listed in Table 1, representing a set of 122 VTEs, which can be categorized into various groups: (i) 69 singlets and 53 triplets; (ii) 83$\pi \rightarrow \pi^*$ and 31$n \rightarrow \pi^*$ valence transitions as well as 8 Rydberg states; and (iii) 4 VTEs smaller than 2 eV, 13 in the 2−3 eV range, 46 in the 3−4 eV range, 39 in the 4−5 eV range, and 20 larger than 5 eV. These subgroups are quite representative of real-life chromophores typically investigated with TD-DFT, ADC(2), or CC2. The underrepresentation of Rydberg ESs in this set, compared to the QUEST database,[52] is a logical consequence of selecting large π-conjugated molecules, in which the majority of the lowest-lying ESs correspond to valence excitations.

3.1.1. On the Accuracy of the TBEs. While CC3 demonstrated exceptional accuracy for the compounds included in the QUEST database, with a trifling MAE of 0.02 eV,[52] predicting changes in its accuracy for the larger compounds studied here is challenging. Thus, we do not provide an anticipated error bar for the TBEs listed in Table 1, though we are confident that these values are the most trustworthy available to date for the systems depicted in Figure 1.

To delve deeper into the accuracy of the TBEs, a valuable metric is $\%T_1$, which defines the percentage of single-excitation character of the transition. Indeed, systematically increasing the degree of the CC excitation operator would not be the optimal strategy if doubly excited states (characterized by low values of $\%T_1$) were involved.[158,159] Among the 122 cases treated here, 62 show $\%T_1 > 90\%$, indicating that they can be safely viewed as almost pure single excitations. Notably, this includes all 53 triplets, which comes as no surprise.[52,160] Most of the remaining singlet states, i.e., 44, fall in the $90\% > \%T_1 > 85\%$ range. In other words, 106-out-of-122 TBEs are associated with $\%T_1 > 85\%$. For these transitions, both CC3 and CCSDT generally performs extremely well. Indeed, for such transitions we demonstrated that, on the one hand, corrections from quadruples (CC4 or CCSDTQ) are essentially negligible,[48] whereas, on the other hand, second-order multireference methods, e.g., CASPT2 and NEVPT2, are significantly less accurate than CC3 with errors of approximately 0.10−0.13 and 0.02 eV, respectively.[161] Next, 10 states are characterized by $85\% > \%T_1 > 80\%$, for which both CC3 and CCSDT are likely no longer chemically accurate, but probably still superior to CASPT2 (or similar methods), based on our experience.[161,162] Finally, Table 1 includes a few transitions with $80\% > \%T_1 > 75\%$ (6 ESs). In these cases, we expect the present TBEs to be too large, i.e., upper bounds of the exact VTEs, as corrections from quadruples typically downshift such states with a significant double excitation character.[48] For such transitions in rather large compounds, it is difficult to know if the CC3/CCSDT or CASPT2/NEVPT2 would be the most accurate. We can only refer to smaller structures for which indisputable TBEs are at hand.[52,159] For the well-known ^1A_g dark ES of butadiene ($\%T_1 = 75\%$), the CC3 and CCSDT errors, relative to the near-exact VTE, are +0.15 and +0.08 eV, respectively, whereas the CASPT2 and NEVPT2 deviations are +0.22 and +0.18 eV, respectively.[52,159] For the lowest $^1E_{2g}$ ES of benzene ($\%T_1 = 73\%$), the CC3, CASPT2 and NEVPT2 errors are respectively +0.18, +0.12, and +0.32 eV.[159] Consequently, there is no clear indication that multireference values would be systematically more accurate than the present CC-based TBEs for our set of data.

Another strategy to probe CC3's accuracy is to investigate the differences between the CC3 and CCSDT values. Though this approach is not entirely foolproof in assessing the impact of further (quadruple) CC corrections,[48] it hints at the convergence of the CC family of methods. From the 29 singlet ESs for which we could compute this difference in the 6−31+G(d) basis set, it results a MAE of 0.034 eV which we regard as a positive indicator of our TBEs' quality. We note that the use of this small basis set should not be an issue. Indeed, we have shown that eq 2 provides excellent estimates of the actual CCSDT/AVTZ results, with a MAE of 0.005 eV, i.e., the CC3-CCSDT differences seems reasonably insensitive to the basis set size.[48] Figure 2 shows these differences as a function of $\%T_1$. As can be seen, there is no clean relationship between the two parameters, although the two largest deviations correspond to states with $\%T_1 < 85\%$. Another interesting outcome, already noticed for substituted phenyls,[163] is that the CCSDT correction tends to be positive, meaning that the CC3 VTEs tend to be lower than their CCSDT counterparts for large molecules.

3.1.2. Comparisons with Literature Data. Let us now briefly compare the TBEs gathered in Table 1 to previous literature values. While a plethora of TD-DFT data, as well as numerous ADC(2) and CC2 results, are available for many chromophores, we decided to focus on data obtained with higher levels of theory. Likewise, we eschewed including

https://doi.org/10.1021/acs.jctc.4c00906
J. Chem. Theory Comput. 2024, 20, 8152−8174

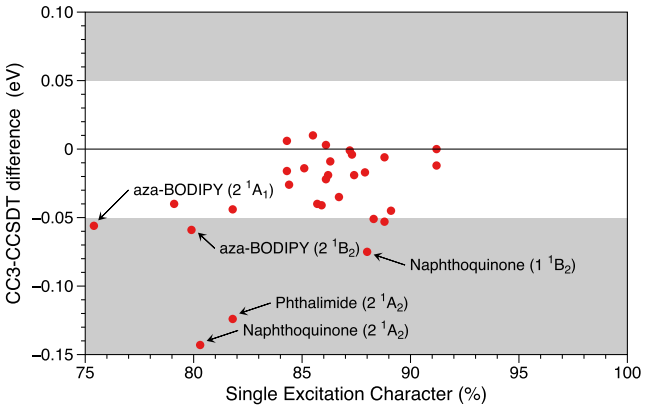

Figure 2. Relationship between the CC3-CCSDT VTE differences (in eV) and the single-excitation character (computed at the CC3 level). The central white zone indicate absolute errors smaller than 0.05 eV. Some outliers are explicitly indicated.

experimental data since the present VTEs do not account for vibronic or solvent effects, making well-grounded comparisons with measured ultraviolet/visible (UV/vis) spectra of solvated dyes unfeasible. For most molecules, we could not find any previous highly accurate estimates of these VTEs.

For anthracene, one can find investigations performed with CASPT2 and DMRG,[164−167] most of them focusing on the singlet−triplet or $L_a - L_b$ gaps. Reference 164 reports the following DMRG-CASPT2/cc-pVTZ(-f) transition energies: 1.73 eV ($^3B_{1u}$), 3.45 eV ($^1B_{1u}$), 3.77 eV ($^1B_{2u}$), 4.97 eV (^1A_g), and 5.00 eV ($^1B_{3g}$). There is globally a fair agreement with the current TBEs that are typically larger, especially for the lowest triplet ES, for which the agreement is especially poor. Note that for the ^1A_g ES of anthracene, we have $\%T_1$ = 75%. Therefore, it is likely that the VTE reported in Table 1 is an upper bound of the exact value.

For aza-BODIPY, the 2.34 eV value obtained at the CASPT2/cc-pVDZ level by Momeni and Brown for the lowest singlet transition[168] is slightly below the present TBE of 2.51 eV.

For azobenzene, one can find MS-CASPT2/6−31G(d),[169] SS-RASPT2/VDZP,[170] and CC3/aug-cc-pVDZ[64] results for the two lowest ESs. These methods respectively return VTEs of 2.86, 2.66, and 2.91 eV for the $n \rightarrow \pi^*$ transitions and 4.17, 3.86, and 4.07 eV for the $\pi \rightarrow \pi^*$ transitions. These previous data are reasonably close to the present estimates of 2.87 and 4.23 eV. We note that the MLCC3/aug-cc-pVDZ results of ref 65. have been determined on a significantly distorted geometry precluding sound comparisons with the present work.

A very complete study of the photophysics of BODIPY was performed by De Vetta and co-workers.[171] For the vertical absorption, they reported CASPT2/ANO-L transition energies of 2.64, 3.78, and 3.87 eV for the three lowest singlet ESs, and 1.92, 3.11, and 3.31 eV for the three lowest triplet ESs. These values are globally in excellent agreement with the TBEs of Table 1 with a MAE of 0.04 eV only. One can also find earlier CASPT2 estimates with smaller basis sets for the lowest singlet transition of BODIPY.[168,172]

The CASPT2/6−31G(d) transition energies to the three lowest singlet ESs are 4.41, 4.66, and 5.13 eV in coumarin.[173] For the first and third states, of $\pi \rightarrow \pi^*$ nature, these values are slightly larger than the present estimates of 4.31 and 4.98 eV, whereas the shift is in the other direction for the second state, corresponding to a $n \rightarrow \pi^*$ transition, for which the present TBE is 4.80 eV.

For the lowest singlet and triplet ESs of both cyclazine and heptazine, which notably exhibit a negative singlet−triplet gap, previous SC-NEVPT2/def2-TZVP estimates reported VTEs of 1.22 eV (singlet) and 1.28 eV (triplet) for cyclazine and 3.26 eV (singlet) and 3.40 eV (triplet) for heptazine.[174] These values are significantly upshifted compared to the present results. There are other multireference values available,[175−177] and one can find a more complete list of literature values for the lowest-lying transitions in Tables 1 and 2 of ref 66.

For tolan, the study of Robertson and Worth provides CASPT2/cc-pVDZ VTEs of 4.71 eV ($^1B_{2u}$), 4.72 eV ($^1B_{3g}$), 5.04 eV ($^1B_{1u}$), and 6.05 eV (^1A_u).[178] The two former are very close to the current TBEs.

3.2. Wave Function Benchmarks.

Having the above-described TBEs at hand, it is natural to assess the performances of lower-level wave function approaches. Indeed, the CC3/aug-cc-pVTZ VTEs listed in Table 1 are at the frontier of today's technical feasibility. Thus, for practical applications, one would clearly wish to use methods that are computationally more affordable. The interested reader can find the full list

Table 2. Statistical Analysis of the Performance of Various Wave Function Methods[a]

	full set			MAE of subsets					
method	MSE	MAE	SDE	singlet	triplet	$\pi \rightarrow \pi^*$	$n \rightarrow \pi^*$	Rydberg	$\%T_1 \geq 85\%$
CIS(D)	0.24	0.24	0.18	0.22	0.28	0.29	0.18	0.06	0.23
CC2	0.03	0.11	0.12	0.09	0.12	0.11	0.10	0.07	0.10
EOM-MP2	0.51	0.51	0.16	0.59	0.41	0.54	0.47	0.40	0.47
CCSD	0.18	0.20	0.16	0.27	0.10	0.18	0.27	0.04	0.16
CCSD(T)(a)*	0.12	0.12	0.07	0.12		0.11	0.15	0.03	0.10
CCSDR(3)	0.11	0.11	0.07	0.11		0.11	0.14	0.03	0.09
CCSDT-3	0.08	0.08	0.05	0.08		0.08	0.11	0.01	0.07
SOS-ADC(2)[TM]	0.22	0.22	0.11	0.21	0.24	0.20	0.28	0.24	0.21
SOS-CC2	0.26	0.26	0.12	0.25	0.28	0.22	0.38	0.17	0.24
SCS-CC2	0.19	0.19	0.07	0.17	0.21	0.18	0.22	0.09	0.18
SOS-ADC(2)[QC]	0.01	0.09	0.11	0.10	0.06	0.08	0.08	0.12	0.08
ADC(2)	−0.01	0.12	0.15	0.11	0.14	0.10	0.21	0.04	0.12
ADC(3)	−0.06	0.20	0.22	0.18	0.23	0.18	0.24	0.19	0.19
ADC(2.5)	−0.04	0.06	0.06	0.06	0.06	0.06	0.05	0.06	0.06

[a]All values are in eV.

https://doi.org/10.1021/acs.jctc.4c00906
J. Chem. Theory Comput. 2024, 20, 8152−8174

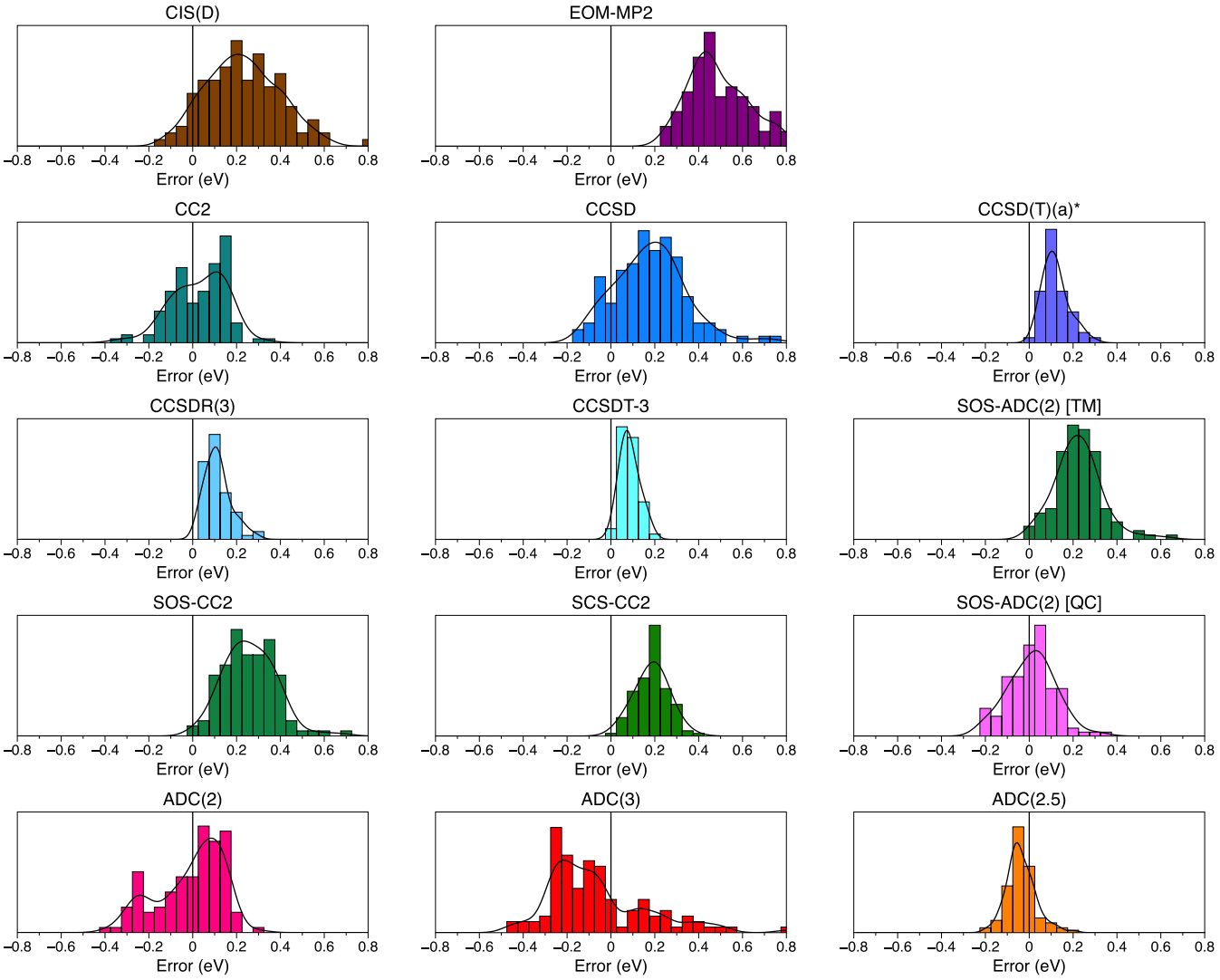

Figure 3. Histograms of the errors as compared to the TBEs for wave function methods considered in the present work.

of raw data in the SI for the 14 wave function methods tested here. In Table 2, we report the results of the statistical analysis: mean signed error (MSE), MAE, and standard deviation of the errors (SDE), together with the MAE obtained for various subgroups of ESs. In Figures 3, S1, and S2, histograms representing the distribution of these errors are available. It should be recalled that: (i) there are only 8 Rydberg transitions in our set; (ii) CCSD(T)(a)*, CCSDR(3), and CCSDT-3 have been implemented for singlet ESs only; and (iii) for some of the most expensive levels of theory [CCSDT-3 for instance], we were not able to obtain all possible VTEs despite our efforts.

In the rightmost column of Table 2, we provide the MAEs obtained for ESs with a single-excitation character, as defined by $\%T_1 \geq 85\%$. As discussed above, we anticipate a very small CC3 error for the vast majority of these states.[48] As can be seen, the MAEs obtained for this subset are only slightly smaller than their counterparts determined on the full set: the typical variations are below 0.04 eV and the methodological trends are preserved. Therefore, we have chosen to perform the following analyses using the entire set of TBEs.

Both CIS(D) and EOM-MP2 provide quite poor transition energies, with a clear overshooting trend as well as large SDEs. This is no surprise.[52,53,75,78,163,179,180] Practically, these approaches are therefore of limited interest: their performances are not clearly superior to the best GHs, while they appear significantly less accurate than several DHs presenting the same $O(N^5)$ formal scaling with system size (vide infra). The EOM-MP2 MAE of 0.51 eV is much larger than its QUEST counterpart of 0.22 eV, and even exceeds the MAE obtained for molecules encompassing 7−10 non-H atoms belonging to the QUEST database (0.42 eV).[52] This indicates that the EOM-MP2 error continues to grow with system size. Nevertheless, in the present set, this overestimation remains relatively systematic, as evidenced by the SDE. In contrast, CIS(D) shows errors in the 0.2−0.3 eV range for all molecular sizes. In other words, it is less affected by the physical extent of the investigated compounds. These errors are notably smaller for both Rydberg and $n \rightarrow \pi^*$ transitions than for $\pi \rightarrow \pi^*$ excitations, consistently with earlier findings.[52]

For the present set of real-life dyes, CC2 emerges as particularly robust with a small MSE, an attractive SDE of 0.12 eV (indicating quite systematic errors), and MAE close to 0.10 eV for all ES families. Interestingly, based on QUEST, we found that the MAE of CC2 is 0.16 eV,[52] but this larger value was mostly driven by the small compounds. Indeed, the MAE

https://doi.org/10.1021/acs.jctc.4c00906
J. Chem. Theory Comput. 2024, 20, 8152−8174

is 0.11 eV for the 7−10 (non-H) atom molecules of QUEST, hinting that the convergence of the CC2 error with system size is likely reached. Nevertheless, one notes a bimodal distribution of the CC2 errors in Figure 3. As can be seen in Figure S1, this originates from the tendency of CC2 to underestimate (overestimate) the VTE of both Rydberg and $n \rightarrow \pi^*$ ($\pi \rightarrow \pi^*$) ESs, which might cause issues if a balanced description of all state types is required. For comparisons, the MAE and SDE of CC2 were found to be 0.07 and 0.09 eV, respectively, in the study of Winter and co-workers,[77] who selected 0−0 experimental energies (for the lowest-lying ESs) as references. We believe that our statistical indicators are slightly higher due to the inclusion of more challenging (higher-energy) ESs in our set.

As discussed in many works,[52,53,77,78,103,163,179−182] ADC(2) does provide a rather similar accuracy as CC2. However, ADC(2) seems slightly less effective than its CC counterpart here, as evidenced by the higher values of the statistical indicators for most ES subgroups considered in Table 2, especially the $n \rightarrow \pi^*$ transitions for which the advantage of CC2 over ADC(2) is clear, since ADC(2) more significantly underestimates the VTEs of those transitions than CC2 (See Figures S1 and S2). This finding differs from the one of ref 52. but parallels the outcomes of Winter and co-workers,[77] who reported a MAE of 0.08 eV and a SDE of 0.12 eV for ADC(2).

Even though the overestimation tendency of CCSD is well-documented,[52,53,160,163,182−186] the MSE (0.18 eV) and MAE (0.20 eV) of Table 2 are surprisingly large, with an obvious unbalanced nature. In particular, the CCSD positive bias is markedly larger for singlets than for triplets (Figure S1). It is also larger for $n \rightarrow \pi^*$ than for $\pi \rightarrow \pi^*$ transitions, though in that case the error patterns seem better than their CC2 counterparts. What was less expected is the large SDE of 0.16 eV, which exceeds its CC2 counterpart of 0.12 eV. Indeed, the reverse SDE trend was noticed in QUEST,[52] CCSD delivering more systematic errors than CC2. In light of these outcomes, the interest in using CCSD rather than CC2 for applications on large compounds seems difficult to justify in general. Adding perturbative corrections for the missing triple excitations helps, with SDE well below 0.10 eV for both CCSD(T)(a)* and CCSDR(3). The MSEs of these two similar methods remain firmly positive, though. Unfortunately, this confirms[52,163] that these two schemes become less effective when one considers larger molecules as they cannot downshift the CCSD VTEs enough. To solve this issue, one can turn to iterative triples with CCSDT-3, but this expensive method shares with CC3 the unpleasant $O(N^7)$ scaling with system size. Note that CCSDT-3 still overestimates our TBEs, albeit by a small acceptable margin.

As originally reported by us,[104] ADC(3) does not improve upon ADC(2), while ADC(2.5), where one simply averages the ADC(2) and ADC(3) VTEs,[52,105,163] appears again to be a relatively affordable $O(N^6)$ approach providing accurate results. Figure S2 clearly shows that the error patterns of ADC(2) and ADC(3) are mirrored for the different types of ESs, explaining the success of ADC(2.5). Indeed, all statistical errors of ADC(2.5) are close to 0.06 eV and it impressively outperforms both CCSD(T)(a)* and CCSDR(3) on the present set, with an absolute accuracy comparable to the one of CCSDT-3, but with an underestimation trend.

Briefly, the most effective spin-scaled approach evaluated here is likely SOS-ADC(2) with the QC parameters,[101] which delivers an accuracy comparable to the one of CC2, for the same formal scaling but with a smaller prefactor. SCS-CC2 (with the TM parameters) yields a very small SDE but at the cost of a clear overshooting trend, a conclusion paralleling previous studies.[52,53,75,78,163,187,188] Both the SOS-ADC(2) and SOS-CC2 with TM parameters appear as less reliable options for the current set. All tested spin-scaled methods also provide reasonably balanced error patterns for singlets and triplets (Figure S2), which is likely advantageous when estimating singlet−triplet gaps.

3.3. TD-DFT and BSE/*GW* Benchmarks. *3.3.1. Gauge Invariance Correction.* As mentioned in Section 2, one can include gauge invariance corrections in TD-DFT calculations involving (hybrid) meta-GGA XCFs. The impact of these corrections was carefully studied and quantified in previous works.[136−138] As enforcing the TDA breaks gauge invariance, it has been argued that applying the gauge corrections at the TDA-DFT level is not necessarily well-grounded.[137] Nevertheless, we have found that the magnitude of the corrections obtained with TDA-DFT and "full" TD-DFT for a given transition are extremely similar (see Figures S3 and S4 in the SI).

Histograms of the changes in VTEs induced by the gauge invariance corrections can be found in Figure 4 for M06, M06−2X, and M06-SX. We note that the corrections are positive with the first two XCFs (i.e., they tend to increase the

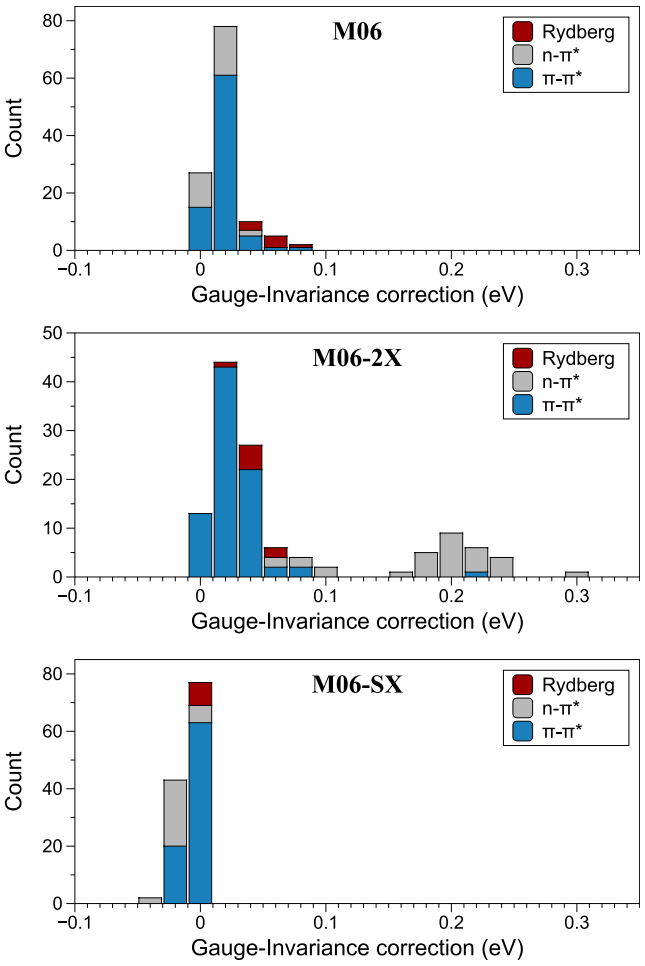

Figure 4. Impact of the gauge invariance corrections for various functionals at the TD-DFT level.

https://doi.org/10.1021/acs.jctc.4c00906
J. Chem. Theory Comput. 2024, 20, 8152−8174

VTEs) but are negative for M06-SX. This trend was expected for M06 and M06−2X, and a rationale for the sign of the correction can be found elsewhere.[136] The average changes are negligible with both M06 (+0.02 eV on average) and M06-SX (−0.01 eV on average). These values hold for both TDA-DFT and TD-DFT. With M06, the increase is slightly larger for the Rydberg ESs (+0.05 eV on average) than for the valence transitions (+0.02 eV for $\pi \rightarrow \pi^*$ and +0.01 eV for $n \rightarrow \pi^*$), whereas variations are always minimal for M06-SX. The impact of the gauge invariance corrections becomes more significant for M06−2X, with average variations of +0.03 eV ($\pi \rightarrow \pi^*$), +0.18 eV ($n \rightarrow \pi^*$), and +0.04 eV (Rydberg). We could not detect any significant difference between singlet and triplet ESs regarding the magnitude of these corrections. The M06−2X values are very similar to the one reported by Grotjahn et al. for smaller molecules but with the same XCFs: +0.04 eV ($\pi \rightarrow \pi^*$) and +0.17 eV ($n \rightarrow \pi^*$).[136] There is however one clear outlier in our set: the ^1A_u $\pi \rightarrow \pi^*$ transition of tolan that undergoes a change of +0.17 eV (TDA-DFT) or +0.22 eV (TD-DFT). This can be explained by the fact that this transition involves orthogonal (nonoverlapping) π and π^* orbitals, and essentially resembles a $n \rightarrow \pi^*$ transition in terms of electron density reorganization. Again, this conclusion fits the one of ref 136.

3.3.2. G_0W_0 vs evGW. To perform a BSE calculation, one must start by computing the *GW* quasiparticle energies and the static limit of the screened Coulomb potential. However, there are many ways of performing *GW* calculations.[153,154,189−193] The impact on the subsequent BSE VTEs has been previously assessed for other sets of compounds.[28,194,195] Here, we compare the two most straightforward and computationally affordable schemes, namely, the one-shot G_0W_0 and the partially self-consistent ev*GW* schemes. Histograms of the differences between the two methods can be found in Figure 5 whereas additional data are given in Table S26 and Figure S13 of the SI.

Obviously, the starting KS (or HF) quantities significantly impact the differences between the ev*GW* and G_0W_0 results, hence the BSE VTEs. It is well-known that HF overlocalizes the orbitals in π-conjugated compounds, which results in overestimated fundamental gaps. This error cannot be fully corrected by the perturbative G_0W_0 scheme. This is why the BSE/ev*GW*@HF VTEs are logically lower than their BSE/G_0W_0@HF counterparts by −0.10 eV on average. The correlation between the error on the highest occupied molecular orbital−lowest unoccupied molecular orbital (HOMO−LUMO) gap at the *GW* level, and the error on the resulting BSE neutral singlet excitation energies, were clearly documented in ref 190. In contrast, ev*GW* induces a large increase of the BSE excitation energies when starting from PBE0, by +0.36 eV on average. This hints that the PBE0 gaps are too small, well corrected at the ev*GW* level, while still somehow underestimated at the nonself-consistent G_0W_0@PBE0 level. Finally, we also find a positive correction, albeit significantly smaller (+0.09 eV), when initiating the BSE/ev*GW* calculations with CAM-B3LYP orbitals and energies.

From Figure 5, it is also clear that as for the gauge effects described in Section 3.3.1, the impact of ev*GW* depends on the nature of the considered transition: it is (relatively) mild for Rydberg transitions, moderate for $\pi \rightarrow \pi^*$ transitions and large for the $n \rightarrow \pi^*$ ES. In contrast, Figure S13 demonstrates that the differences between the two *GW* procedures are almost independent of the application of the TDA.

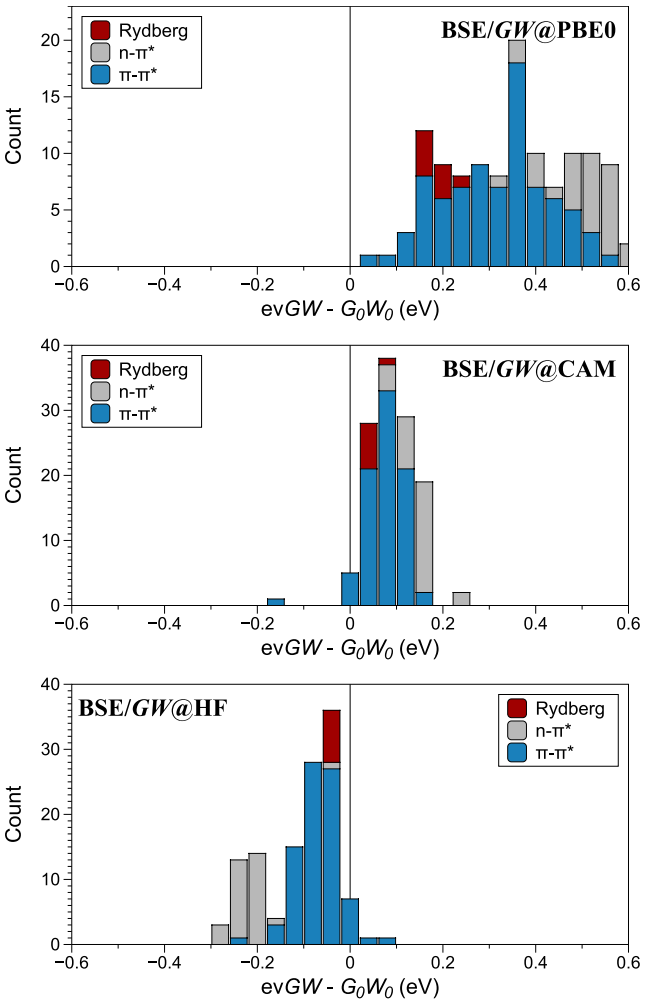

Figure 5. Histograms of the difference between (full) BSE/*GW* results obtained on the basis of ev*GW* and G_0W_0 quasiparticle energies for three different starting points.

3.3.3. Effect of the TDA. As expected,[86,137,151,195−199] applying the TDA induces an almost systematic increase in the transition energies, a statement holding true for both TD-DFT and BSE/*GW*. The few exceptions are related to states characterized by a significant orbital mixing with an admixture modified by the application of the TDA. ωB97X-2 seems particularly prone to deliver negative TDA corrections. We present histograms of the TDA corrections for B3LYP, SOGGA-11X, M06-SX, CAM-B3LYP, ωB97, cLH20t, as well as two BSE/*GW* schemes in Figure 6. The graphs for the other XCFs as well as Tables of statistical data can be found in Sections S5.2 and S6.2 of the SI.

For all XCFs and for both TD-DFT and BSE, the impact of the TDA is negligible for Rydberg ESs (typically less than 0.01 eV), rather small for $n \rightarrow \pi^*$ transitions (ca. 0.05 eV), and significant for $\pi \rightarrow \pi^*$ excitations (from 0.1 to 0.3 eV depending on the XCF). The relative ranking of the ESs can therefore be affected. As expected as well, for the vast majority of the tested XCFs, the upshifts induced by the TDA are larger for the triplet than for the singlet transitions (Figure 7). For TD-DFT, we could find only one clear exception to this general rule, namely cLH12ct-SsirPW92, whereas the average variations are essentially equivalent for ESs of both spin symmetries with both M06-2X and M08-HX. Consistent with

https://doi.org/10.1021/acs.jctc.4c00906
J. Chem. Theory Comput. 2024, 20, 8152−8174

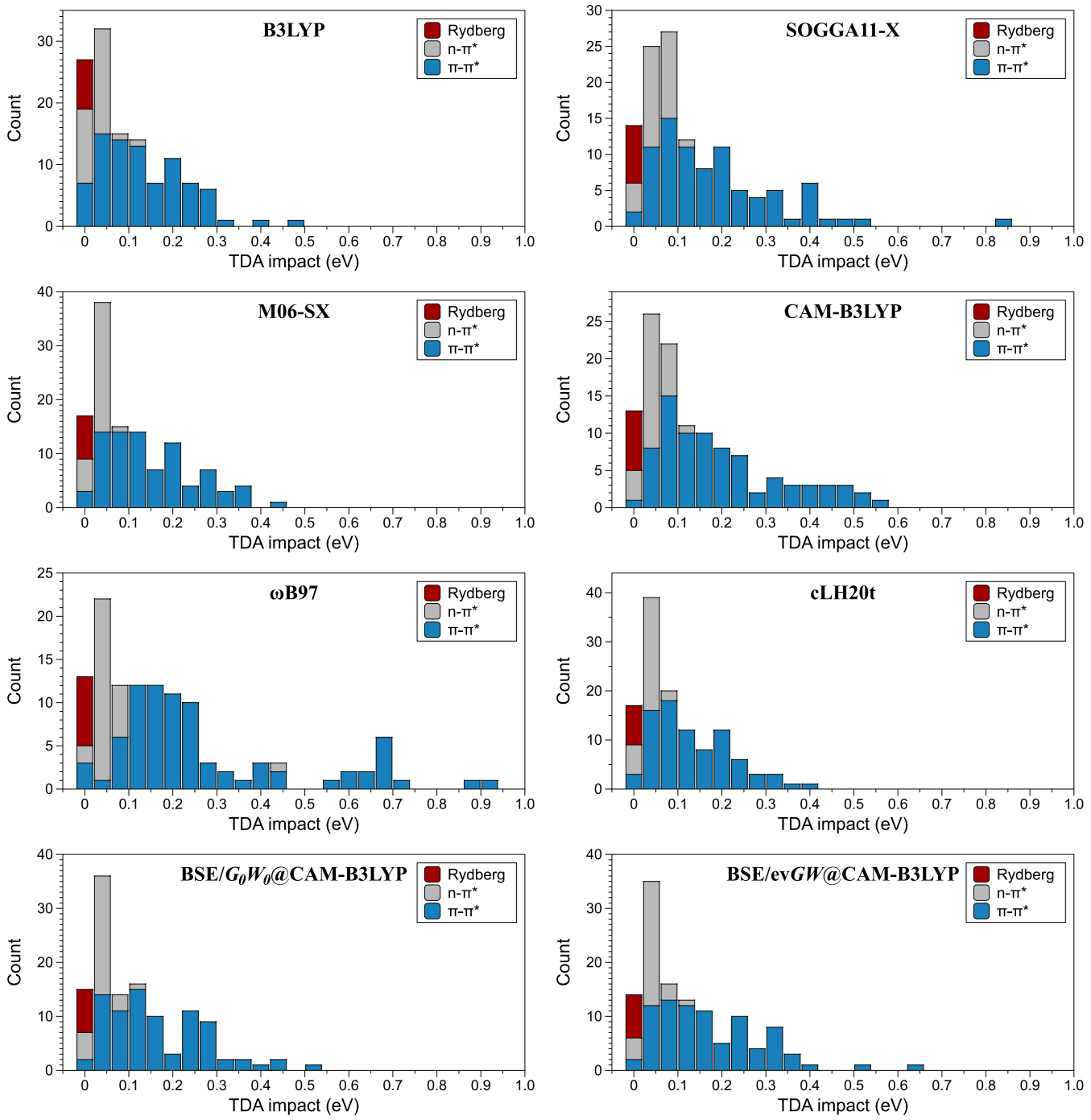

Figure 6. Impact of the application of the TDA on the VTEs (in eV) for selected TD-DFT and BSE/*GW* schemes. Note the difference in scaling of the vertical axes.

an earlier work,[199] the picture is more contrasted in BSE/*GW* with 3-out-of-6 schemes leading to larger corrections for singlet than for triplet transitions (Figure 7 and Table S27). In TD-DFT, the average upshifts for the singlets are +0.09/+0.10 eV for the least TDA-sensitive XCFs, that is, the GHs including a small fraction of exact exchange (EXX), the LHs, and several DHs (B2PLYP, PBE0-DH, PBE-QIDH, and ωB97X-2). The impact of the TDA on the singlet ESs becomes slightly larger for RSHs and some DHs, e.g., +0.13 eV for M11, ωB97, and RSH-0DH. Nevertheless, the changes are rather systematic and also quite insensitive to the selected functional: for a given molecule, the ESs that are strongly affected by the TDA are the same irrespective of the chosen XCF. The same holds for BSE/*GW* with an average increase of the singlet energies of +0.11/+0.12 eV depending on the selected variant. As expected,[137] the picture is significantly different for the triplet ESs in TD-DFT, with corrections clearly increasing with the amount of EXX and average energetic shifts becoming very large for some XCFs, such as LC-ωPBE (+0.36 eV) and rCAM-B3LYP (+0.52 eV). SCAN0 is an outlier with an average increase of +0.29 eV, despite a rather small fraction of EXX (25%). The peculiar behavior of SCAN0 was reported earlier.[137] Consistent with an earlier observation,[200] the LHs seems relatively unaffected by the use of the TDA. Yet, the increase of

https://doi.org/10.1021/acs.jctc.4c00906
J. Chem. Theory Comput. 2024, 20, 8152−8174

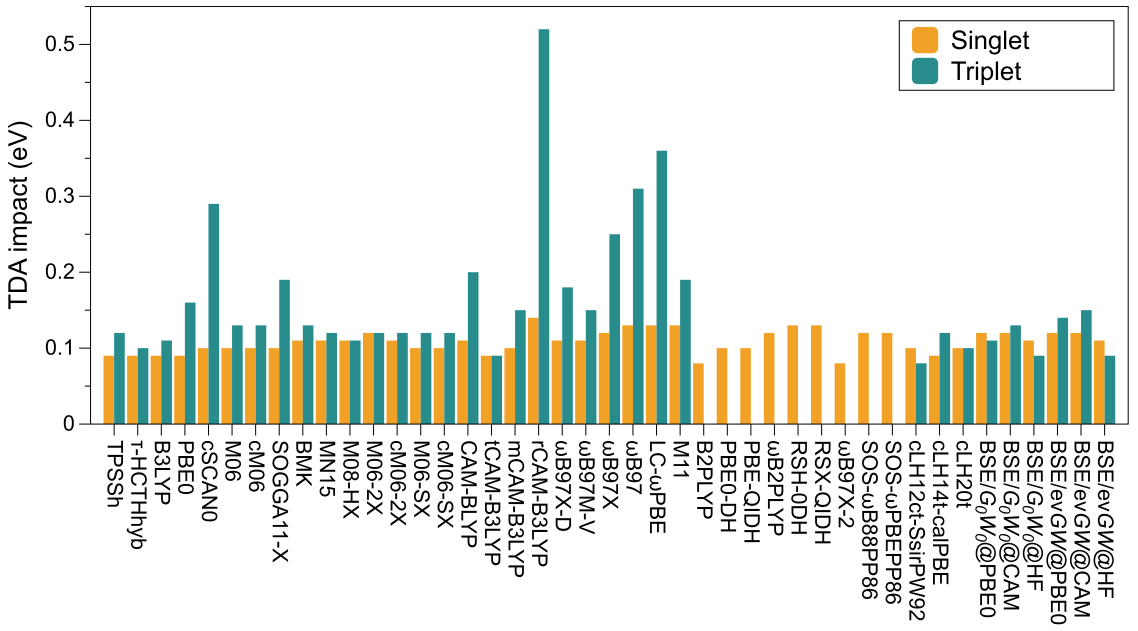

Figure 7. Average impact of the application of the TDA (in eV) for singlet and triplet ESs for various computational schemes based on TD-DFT and BSE/*GW*.

triplet VTEs, ranging from +0.09 to +0.12 eV for the three tested LHs, is rather similar to the one obtained with B3LYP, namely +0.11 eV. For the triplet ESs, the increase in the BSE VTEs seems smaller with G_0W_0 than ev*GW* and smaller when starting from HF than KS (PBE0 and CAM-B3LYP) eigenstates. Nevertheless, the impact of the TDA on the triplet transition energies appears slightly smaller with BSE@CAM-B3LYP than with TD-DFT@CAM-B3LYP (as evidenced by the comparison of Tables S23 and S26).

At this stage, we believe that it is not possible to conclude if enforcing the TDA is beneficial in general. Therefore, we benchmark both flavors in the following.

3.3.4. TD-DFT vs TBE. We now turn toward the assessment of all XCFs against the TBEs. Full data can be found in Tables S24−S25 (for TD-DFT) and S29 (for BSE) in the SI, together with histograms of the errors, whereas a graphical representation of the MSEs, MAEs, and SDEs can be found in Figure 8. We start our analysis below by concentrating on the TD-DFT data before turning our attention to the BSE/*GW* results in the next Section.

As expected, for the GHs, the evolution of the TD-DFT MSEs roughly follows the percentage of EXX:[13] it is negative for XCFs with low EXX percentage and becomes close to zero from 40% of EXX. The impact of applying the TDA and thus upshifting all values is also clear. For example, it decreases the MSE of PBE0 from −0.28 to −0.16 eV while increasing its M06-2X counterpart from +0.03 to +0.14 eV. Within the TDA, all RSHs have positive MSEs, except for tCAM-B3LYP and mCAM-B3LYP, whereas in TD-DFT, ωB97X-D shows a tiny average deviation of −0.02 eV. Two of the tested LHs, namely, cLH12ct-SsirPW92 and cLH20t, also show small negative (positive) MSEs with TD-DFT (TDA-DFT). Among the tested DHs, three of them (PBE0-DH, SOS-ωB88PP86, and SOS-ωPBEPP86) show absolute MSEs smaller than 0.10 eV, irrespective of the application of the TDA.

Let us now turn to the MAEs. The MAEs for each ES subsets can be found in Tables S24 and S25 of the SI. For the most accurate XCFs, considering only transitions with a dominant single-excitation character ($\%T_1 \geq 85\%$) slightly decreases the MAEs, which is the expected trend since adiabatic TD-DFT is not equipped to describe properly ESs having a partial double-excitation character. In contrast, the relative deviations obtained for $\pi \rightarrow \pi^*$, $n \rightarrow \pi^*$, and Rydberg ESs is strongly dependent on the XCF, with a magnified XCF-sensitivity for the latter type of states.[137] Among the GHs, the smallest MAEs are obtained for TD-cM06-2X and TD-M06-2X, the former functional delivering an error as small as 0.14 eV for the transitions showing $\%T_1 \geq 85\%$, a rather remarkable result. It is noteworthy that, with these two XCFs, the final error is driven by the singlet (and not triplet) ESs. Comparisons for smaller molecules using Thiel's set have indeed highlighted TD-M06-2X as a valuable method for singlet−triplet transitions.[201] When applying the TDA, the smallest GH MAE is obtained with BMK: 0.19 or 0.16 eV for the $\%T_1 \geq 85\%$ transitions. Among the RSHs, the smallest MAEs are 0.21 eV for TD-ωB97M-V and 0.19 eV with TDA-(c)M06-SX and TDA-CAM-B3LYP. Globally, the long-range corrected XCFs with large attenuation parameters (ωB97 and LC-ωPBE) are significantly less satisfying, but the present set does not contain clear CT ESs that might require such XCFs.[72] Among the three tested LHs, cLH20t appears to be the most accurate for the present data set with MAEs of 0.19 eV (TD-DFT) and 0.15 eV (TDA-DFT). The accuracy of TD-DFT/TDA-DFT can be also improved by using the more computationally demanding DHs with, e.g., MAEs of approximately 0.15 eV for PBE0-DH and PBE-QIDH. Even smaller values are obtained with XCFs designed to reproduce transition energies, namely SOS-ωB88PP86 and SOS-ωPBEPP86, the later providing a quite astonishing MAE of 0.10 eV when combined with the TDA. However, relatively poor estimates are obtained for the few Rydberg transitions considered here.

An important feature is consistency and this is measured by the SDE which assesses the systematic character of the errors. Gratifyingly, in both TD-DFT and TDA-DFT, the smallest SDEs are obtained with cM06-2X in the GH series and

https://doi.org/10.1021/acs.jctc.4c00906
J. Chem. Theory Comput. 2024, 20, 8152−8174

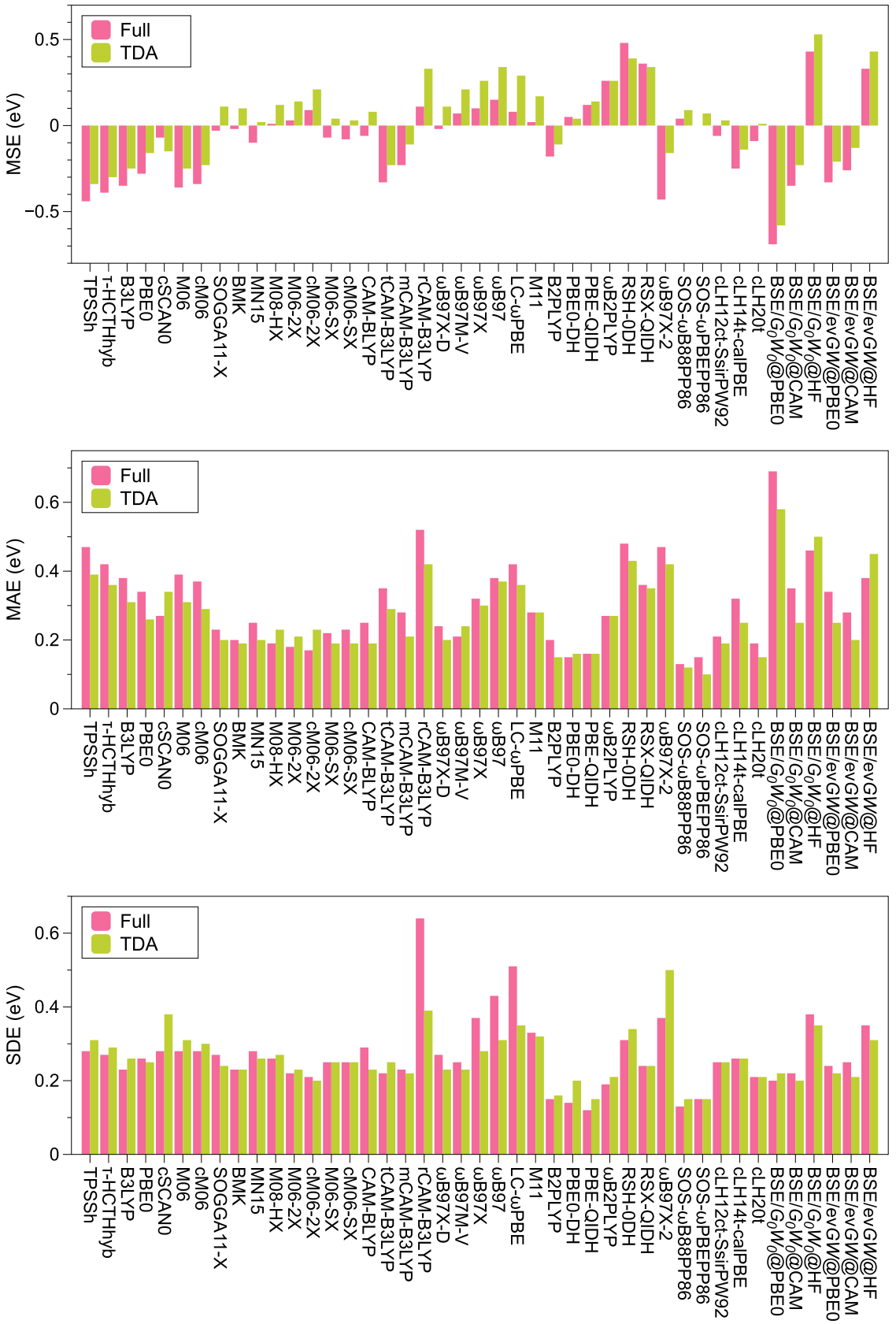

Figure 8. From top to bottom: MSEs, MAEs, and SDEs (in eV) for all XCFs using both the full (pink) and the TDA-based (green) approaches for all evaluated TD-DFT and BSE/*GW* models.

cLH20t in the LH series: the MAE and SDE performances parallel each other for these two groups of XCFs. This is not the case for the RSHs at the TD-DFT level, since tCAM-B3LYP, which was tuned to reproduce transition energies in

https://doi.org/10.1021/acs.jctc.4c00906
J. Chem. Theory Comput. 2024, 20, 8152−8174

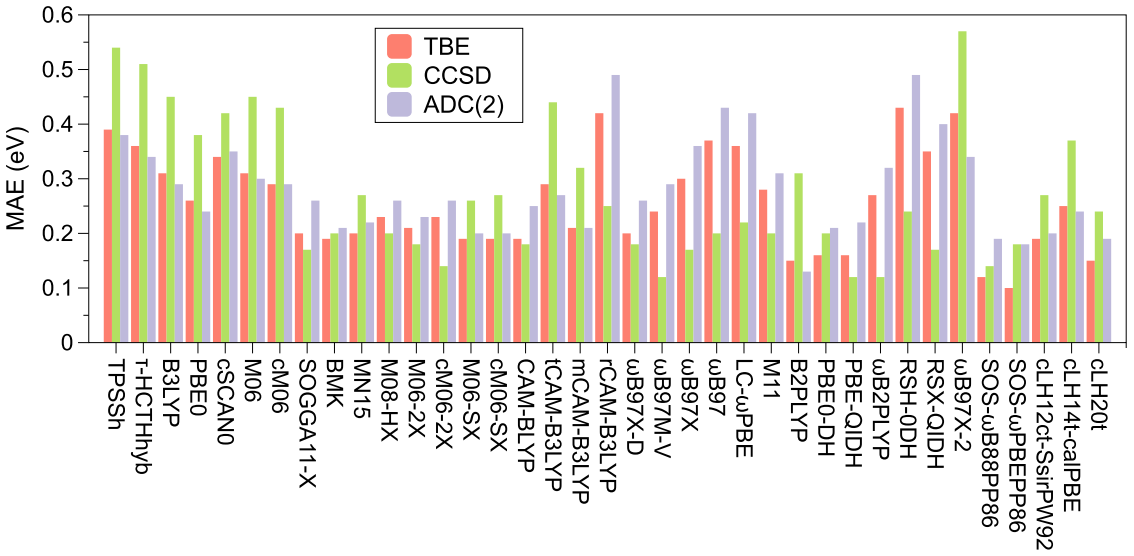

Figure 9. MAEs (in eV) obtained at the TDA-DFT level using the TBE (red), CCSD (green), and ADC(2) (purple) data as reference for various XCFs.

diarylethene photochromes, delivers a small SDE of 0.22 eV, despite a rather large MAE of 0.35 eV. Within the TDA, the smallest RSH SDEs are reached with mCAM-B3LYP, CAM-B3LYP and ωB97X-D. In the DH series, PBE-QIDH provides a SDE of 0.12 eV at the TD-DFT level (a set that does not contain triplets, however). When enforcing the TDA, a SDE of 0.15 eV can be obtained with the same functional, as well as with the already mentioned SOS-ωB88PP86 and SOS-ωPBEPP86 XCFs.

In short, it appears possible to select GHs, RSHs, and LHs providing an accuracy around 0.15−0.20 eV for the present dataset, the best performing schemes being likely TD-cM06-2X and TDA-cLH20t. To reach more accurate estimates, DHs are relevant alternatives, with MAEs and SDEs not exceeding 0.15 eV with both SOS-ωB88PP86 and SOS-ωPBEPP86. The performances of these two XCFs are clearly superior to the one obtained with CIS(D), and rather similar to the one of ADC(2) and CC2. Given this outcome, it is quite evident that benchmarking DH XCFs using "reference" data produced with these second-order methods is not well-founded (vide infra).

Compared to the recent results of refs 137,146, where the original QUEST data were used to benchmark XCFs within the TDA, one notices that the conclusions regarding the most accurate XCFs are quite similar, with, on the one hand, valuable performances of BMK, M06-SX, ωB97X-D, SOGGA11-X, and CAM-B3LYP (within the TDA)[137] and, on the other hand, excellent results obtained with PBE-QIDH, SOS-ωB88PP86 and SOS-ωPBEPP86 in the DH category.[146] The order of magnitude of the errors reported in these different contributions is also reasonably consistent with the current ones, which is reassuring and hints that the conclusions are rather robust (for organic compounds). In an older assessment relying on Thiel's set,[7] the conclusions differed with, for instance, PBE0 providing a MAE significantly smaller than BMK (0.24 vs 0.34 eV as compared to 0.34 vs 0.20 eV here). Likewise, for a given XCF, earlier benchmarks have typically delivered larger MAEs than the ones reported here.[7,183,202−204] For instance, ref 183, which relied on experimental references, reported a MAE of 0.55 eV for TD-PBE0 as compared to 0.34 eV here. Likewise, Gordon's analysis, which also considers experimental reference energies, reported a MAE of 0.59 eV for CAM-B3LYP, as compared to 0.25 eV in the present case.[204] This clearly indicates that the quality of the reference energies is crucial for providing a reliable assessment of these methods. We here recall that comparisons between theoretical VTEs and experimental values are inherently biased. Nevertheless, previous benchmark studies already highlighted BMK[202] and M06-2X[201,203,204] as adequate XCFs for ES calculations within the TD-DFT and/or TDA-DFT formalisms.

3.3.5. BSE/GW vs TBE. Let us now discuss BSE/*GW*. The plots displayed in Figure 8 and the data of Table S29 indicate that HF starting quantities are not recommended: they lead to strong overestimations of the VTEs with MSEs larger than 0.3 eV irrespective of the applications of the TDA and/or the selection of ev*GW* or G_0W_0. Large errors are obtained for all subsets of ESs. Although they lead to negative MSEs, KS orbitals are clearly more adequate for the present systems. Globally, the more rudimental G_0W_0 scheme is detrimental to the final accuracy, especially with PBE0 since the VTEs are largely underestimated, consistent with earlier benchmarks performed on Thiel's set.[28,190,194] G_0W_0 requires XCFs with a large share of EXX as, for example, CAM-B3LYP.[190] The smallest MAE and SDE, both of 0.20 eV, are reached with TDA-BSE/ev*GW*@CAM-B3LYP. Such deviations can likely be viewed as rather large since several XCFs deliver more accurate results when used in TD-DFT calculations.

Consistent with earlier findings,[28,190,195,199] we have found that BSE/*GW* provides an unbalanced treatment of singlet and triplet ESs. Indeed, three BSE schemes, namely BSE/ev*GW*@CAM-B3LYP, TDA-BSE/ev*GW*@PBE0, and TDA-BSE/ev*GW*@CAM-B3LYP, deliver MAEs smaller than 0.15 eV for the singlet transitions, with an average error as small as 0.11 eV for the latter approach. For comparison, the most effective XCFs among the GHs, RSHs, and LHs produce significantly larger MAEs for the same subset (0.18 eV for TD-cLH20t and 0.19 eV for TDA-cLH20t), whereas even the best DH (0.13 eV for TDA-SOS-ωPBEPP86) cannot outcompete this tiny MAE. For the same BSE schemes, the MAE on the triplets increases to 0.48, 0.40, and 0.33 eV, respectively, with a significant improvement associated with the TDA. The stability of the BSE/ev*GW* data, despite the significant differences between

https://doi.org/10.1021/acs.jctc.4c00906
J. Chem. Theory Comput. 2024, 20, 8152−8174

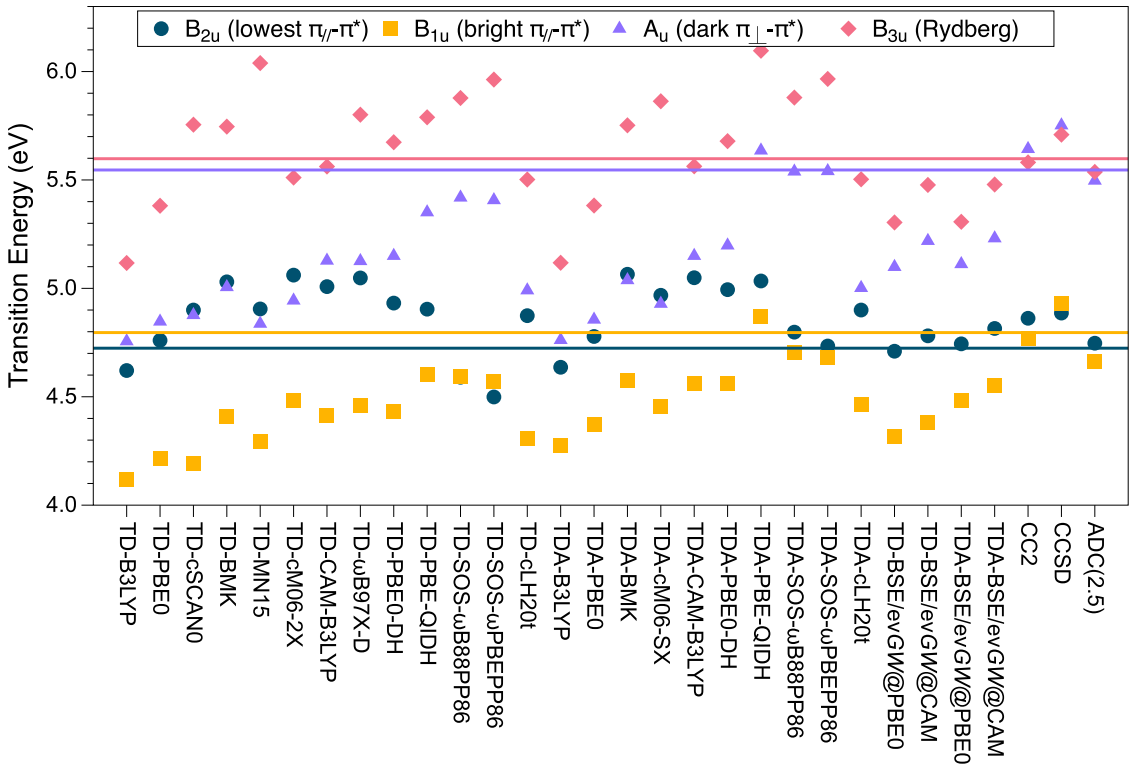

Figure 10. Excitation energies of the four lowest ungerade singlet ESs of tolan computed with various computational schemes. The horizontal lines correspond to the TBE associated with each state as reported in Table 1.

the KS starting points, from the PBE0 GH to the CAM-B3LYP RSH, indicates the advantage of the partially self-consistent ev*GW* scheme that dramatically limits the starting point dependency. This is also clearly seen in the data given in Table S28 and Figure S15 in the SI that demonstrate that the impact of starting with CAM-B3LYP instead of PBE0 is rather small with BSE/ev*GW* (+0.08 eV), but becomes significant with BSE/G_0W_0 (+0.34 eV). For comparison, the corresponding TD-DFT shift is +0.22 eV. In short, we confirm that BSE/ev*GW* can be a valuable alternative to TD-DFT for singlet ESs (only) since the resulting errors are similar to those of ADC(2) and CC2. This conclusion is in line with the results obtained in ref 78. Optimally tuned RSHs,[195] fully self-consistent *GW* schemes[28] or hybrid BSE/TD-DFT approaches,[205] are three possible pathways to improve the description of the triplet ESs within the BSE formalism.

3.4. Further Discussion. Another aspect that we already briefly evoked in Section 3.3.4 is the importance of accurate references for benchmarking purposes. This central point is illustrated in Figure 9 where we provide the MAEs obtained at the TDA-DFT level considering the entire set of XCFs using the TBE, CCSD, or ADC(2) values as references. We underline that all ESs are present for all methods (both reference and tested approaches), allowing well-grounded comparisons. Obviously, benchmarking TDA-DFT with CCSD references is not a fantastic idea: the MAEs of the GHs with a low EXX percentage significantly increase (e.g., B3LYP's MAE goes from 0.31 to 0.45 eV), whereas the MAEs of RSHs with a large attenuation parameter are strongly underestimated (e.g., ωB97X's MAE goes from 0.30 to 0.17 eV). This is the logical consequence of the tendency of CCSD to overestimate the VTEs, as illustrated in Figure 2. In other words, CCSD favors XCFs with a large amount of EXX, since they exhibit the same overshooting predisposition.

From the wave function results of Table 2, one could argue that opting for ADC(2) as a reference method is a better choice since it presents a more balanced error pattern with a near-zero MSE of −0.01 eV (Table 2). ADC(2) is actually the reference method of the very recent DELFI "oracle" whose aim is to predict the most suitable XCF for a given compound through a machine-learning-based approach.[206] From Figure 9, one indeed notices quite similar MAE patterns for most XCFs when using the TBE or ADC(2) values as references. However, by taking a closer look, one sees that the MAEs predicted for the most accurate XCFs are significantly overshot when one relies on ADC(2). For example, SOS-ωB88PP86's and SOS-ωPBEPP86's MAEs are shifted from 0.12 to 0.19 eV and from 0.10 to 0.18 eV, respectively when replacing the TBEs by the ADC(2) data. Actually, ADC(2) would also incorrectly foresee B2PLYP as the best performing DH with a MAE of 0.13 eV. In other words, ADC(2) can probably be employed to pinpoint poor XCFs, but is likely not accurate enough to highlight the best ones.

As performing an exhaustive benchmark study for a long list of ESs is a rather tedious task (especially in terms of state identification), it might also be useful to have a quick challenging test when, for example, developing new methods or testing new protocols. In Figure 10, we provide, for a representative set of methods, the energies of the lowest four ungerade singlet ESs of tolan. They encompass the lowest-lying and nearly dark $\pi \rightarrow \pi^*$ state (B_{2u}), a very bright $\pi \rightarrow \pi^*$ state (B_{1u}), a Rydberg state (B_{3u}), and the already mentioned state involving a transition between orthogonal $\pi_\perp$ and π^* orbitals (A_u). In short, these four states represent a quite diverse and somehow representative panel. Interestingly, the first two and

https://doi.org/10.1021/acs.jctc.4c00906
J. Chem. Theory Comput. 2024, 20, 8152−8174

last two ESs are (nearly) energetically degenerate according to the data of Table 1. As can be seen in Figure 10, while the three reported wave function approaches reasonably reproduce the energy pattern (albeit with some state inversions), TD-DFT and TDA-DFT calculations based on GHs, RSHs, and LHs provide unsatisfactory results: the bright ES is typically over stabilized, the B_{2u} and A_u ESs are too close in energy, while the Rydberg ES is somehow randomly located. BSE/*GW* also over stabilizes the B_{1u} states but it more correctly separates the B_{2u} and A_u ESs. The DHs also struggle in locating the Rydberg transition (and sometimes the $\pi_\perp\pi^*$ state), though some of them are more successful for the three valence states.

4. CONCLUSIONS

In an effort to extend our dataset of accurate VTEs to larger molecules than those in the original QUEST database, and to address compounds more typical of those modeled in TD-DFT applications, we have determined 122 VTEs in 13 organic chromophores using CC3, and, when possible, CCSDT, to establish reference values. This new set maintains a reasonably good balance between singlet and triplet transitions, as well as between $\pi \rightarrow \pi^*$ and $n \rightarrow \pi^*$ excitations, but includes only 8 Rydberg transitions, making it valence-biased and lacking in CT transitions. Among these 122 VTEs, 106 have a $\%T_1 \geq 85\%$, indicating ESs with strong single-excitation character for which CC3 is particularly well-suited, often delivering chemically accurate results for smaller compounds. Unfortunately, this statement cannot be definitively confirmed here, as CC4, CCSDTQ, and FCI estimates are beyond our current computational capabilities. Therefore, we cannot provide a precise error bar for our TBEs. Nevertheless, it is reasonable to assume that the transition energies listed in Table 1 currently constitute the best theoretical reference values available for the compounds in Figure 1.

With these reference values at hand, we benchmarked more computationally affordable methods. Indeed, CC3 is generally too expensive to be used in practice. To give an order of magnitude, computing the four CC3/AVTZ VTEs of aza-BODIPY took us 29 days of (real) time on a 2Tb/48 cores node, though such timing of course depends on the details of both the implementation and architecture. In our benchmark, we first considered 14 second- and third-order wave function methods. A key finding is that the predictions of CCSD are poorer than those of CC2 and ADC(2) in terms of absolute errors (which was expected) and standard deviations (which differs from results obtained for smaller compounds). The conclusion that CC2 is less consistent than CCSD does not always hold for larger, real-life molecules. While some might view this finding as good news for practical applications, as CC2 is a relatively cheap method (e.g., the same four ESs of aza-BODIPY could be computed in less than 1 h on a standard 128 GB/32 cores node), our data suggest that significant improvements might require much more expensive wave function approaches like CC3 or CCSDT. Correcting CCSD VTEs with perturbative estimates of the triples still does not clearly outperform CC2 in terms of absolute deviation. Consistent with the results obtained in the original QUEST, we found that the ADC(2.5) protocol, which averages ADC(2) and ADC(3) VTEs, is the best performing method among all $O(N^5)$ and $O(N^6)$ wave function methods we tested here, although it suffers from a small, nearly systematic under-estimation trend. In practice however, the ADC(3) calculations will be the bottleneck in the ADC(2.5) protocol.

We have also considered a large set of computationally more effective models, including TD-DFT with many global, range-separated, local, and double hybrid XCF, applied with or without the TDA, as well as various BSE/*GW* models. These methods often require a fraction of the computational effort of their wave function counterparts and are typically used when modeling organic dyes. Gratifyingly, our conclusions for both TD-DFT and BSE/*GW*, both qualitatively and quantitatively, align well with the most recent benchmarks.

Among the GHs, we found that (c)M06-2X and BMK are particularly accurate when performing TD-DFT and TDA-DFT calculations, respectively. These widely available models deliver small MAEs/SDEs and are more accurate for triplet than for singlet transitions. Similar accuracies can be obtained with TDA-CAM-B3LYP or TD(A)-cLH20t. All these approaches provide MAEs slightly below 0.20 eV with an acceptable spread of errors. Further error reduction can be achieved using DHs, with PBE0-DH, PBE-QIDH, SOS-ωB88PP86, and SOS-ωPBEPP86 emerging as the four most accurate, especially the latter two, which deliver very small MAEs close to 0.10 eV for valence transitions (but not for Rydberg transitions).

For BSE/*GW*, we confirmed that partial self-consistency at the ev*GW* level, or the proper tuning of the starting DFT functional, are necessary to achieve reasonable accuracy. The most satisfactory model we tested here, TDA-BSE/ev*GW*@CAM-B3LYP, delivers a smaller MAE than all TD-DFT models we evaluated, including the best DH, for singlet ESs. However, this success comes at the cost of large deviations for triplet ESs.

In conclusion, although the present database is inherently biased toward medium-sized π-conjugated organic compounds, we hope the values listed in Table 1 will be useful for testing emerging electronic structure theories for ESs resembling those in real-life quantum chemical applications. These values help bridge the gap between existing high-accuracy VTEs, obtained for more compact molecules, and 0−0 benchmarks, typically limited to the lowest bright ESs. We are currently: (i) adding DNA bases to the QUEST database; and (ii) preparing a review article containing all reference data generated since the first QUEST paper in 2018.

■ ASSOCIATED CONTENT

Supporting Information

The Supporting Information is available free of charge at https://pubs.acs.org/doi/10.1021/acs.jctc.4c00906.

Excited-state characterizations; full list of raw vertical excitation energies; additional statistical data, and geometries (PDF)

Raw data for all states (XLSX)

Summary (XLSX)

■ AUTHOR INFORMATION

Corresponding Authors

Pierre-François Loos − *Laboratoire de Chimie et Physique Quantiques, Université de Toulouse, CNRS, UPS, 31062 Toulouse, France;* orcid.org/0000-0003-0598-7425; Email: loos@irsamc.ups-tlse.fr

Denis Jacquemin − *Nantes Université, CNRS, CEISAM UMR 6230, F-44000 Nantes, France; Institut Universitaire de*

https://doi.org/10.1021/acs.jctc.4c00906
J. Chem. Theory Comput. 2024, 20, 8152−8174

France (IUF), F-75005 Paris, France; orcid.org/0000-0002-4217-0708; Email: Denis.Jacquemin@univ-nantes.fr

Authors

Iryna Knysh − *Nantes Université, CNRS, CEISAM UMR 6230, F-44000 Nantes, France;* orcid.org/0000-0001-8420-9431

Filippo Lipparini − *Dipartimento di Chimica e Chimica Industriale, University of Pisa, 56124 Pisa, Italy;* orcid.org/0000-0002-4947-3912

Aymeric Blondel − *Nantes Université, CNRS, CEISAM UMR 6230, F-44000 Nantes, France*

Ivan Duchemin − *Université Grenoble Alpes, CEA, IRIG-MEM-L Sim, 38054 Grenoble, France;* orcid.org/0000-0003-4713-1174

Xavier Blase − *Université Grenoble Alpes, CNRS, Institut NEEL, F-38042 Grenoble, France;* orcid.org/0000-0002-0201-9093

Complete contact information is available at: https://pubs.acs.org/10.1021/acs.jctc.4c00906

Notes

The authors declare no competing financial interest.

■ ACKNOWLEDGMENTS

This work was supported by the French Agence Nationale de la Recherche (ANR) under Contract No. ANR-20-C.E.29-0005 (BSE-Forces). I.K. received financial assistance from the state within the framework of the EUR LUMOMAT project and the Investissements d'Avenir program ANR-18-EURE-0012. P.-F.L. thanks the European Research Council (ERC) under the European Union's Horizon 2020 research and innovation programme (grant agreement no. 863481) for financial support. This research used resources of the GLiCID Computing Facility (Ligerien Group for Intensive Distributed Computing, 10.60487/glicid, Pays de la Loire, France).

■ REFERENCES

(1) Adachi, M.; Nakamura, S. Comparison of the INDO/S and the CNDO/S method for the absorption wavelength calculation of organic dyes. *Dyes Pigm.* **1991**, *17*, 287−296.

(2) Laurent, A. D.; Adamo, C.; Jacquemin, D. Dye Chemistry with Time-Dependent Density Functional Theory. *Phys. Chem. Chem. Phys.* **2014**, *16*, 14334−14356.

(3) Casida, M. E. Time-Dependent Density-Functional Response Theory for Molecules. In *Recent Advances in Density Functional Methods*; Chong, D. P., Ed.; World Scientific: Singapore, 1995; Vol. *1*, pp 155−192.

(4) Ullrich, C. Time-Dependent Density-Functional Theory: Concepts and Application. In *Oxford Graduate Texts*; Oxford University Press: New York, 2012.

(5) Guillaumont, D.; Nakamura, S. Calculation of the Absorption Wavelength of Dyes Using Time-Dependent Density-Functional Theory (TD-DFT). *Dyes Pigm.* **2000**, *46*, 85−92.

(6) Jacquemin, D.; Perpète, E. A.; Scuseria, G. E.; Ciofini, I.; Adamo, C. TD-DFT Performance for the Visible Absorption Spectra of Organic Dyes: Conventional Versus Long-Range Hybrids. *J. Chem. Theory Comput.* **2008**, *4*, 123−135.

(7) Jacquemin, D.; Wathelet, V.; Perpète, E. A.; Adamo, C. Extensive TD-DFT Benchmark: Singlet-Excited States of Organic Molecules. *J. Chem. Theory Comput.* **2009**, *5*, 2420−2435.

(8) Dierksen, M.; Grimme, S. The Vibronic Structure of Electronic Absorption Spectra of Large Molecules: A Time-Dependent Density Functional Study on the Influence of *Exact* Hartree-Fock Exchange. *J. Phys. Chem. A* **2004**, *108*, 10225−10237.

(9) Improta, R.; Barone, V.; Santoro, F. Ab initio calculations of absorption spectra of large molecules in solution: coumarin C153. *Angew. Chem., Int. Ed.* **2007**, *46*, 405−408.

(10) Avila Ferrer, F. J.; Cerezo, J.; Stendardo, E.; Improta, R.; Santoro, F. Insights for an Accurate Comparison of Computational Data to Experimental Absorption and Emission Spectra: Beyond the Vertical Transition Approximation. *J. Chem. Theory Comput.* **2013**, *9*, 2072−2082.

(11) Cerezo, J.; Santoro, F. Revisiting Vertical Models To Simulate the Line Shape of Electronic Spectra Adopting Cartesian and Internal Coordinates. *J. Chem. Theory Comput.* **2016**, *12*, 4970−4985.

(12) Santoro, F.; Jacquemin, D. Going Beyond the Vertical Approximation with Time-Dependent Density Functional Theory. *WIREs Comput. Mol. Sci.* **2016**, *6*, 460−486.

(13) Laurent, A. D.; Jacquemin, D. TD-DFT Benchmarks: A Review. *Int. J. Quantum Chem.* **2013**, *113*, 2019−2039.

(14) Loos, P. F.; Scemama, A.; Jacquemin, D. The Quest for Highly-Accurate Excitation Energies: A Computational Perspective. *J. Phys. Chem. Lett.* **2020**, *11*, 2374−2383.

(15) Goerigk, L.; Moellmann, J.; Grimme, S. Computation of Accurate Excitation Energies for Large Organic Molecules with Double-Hybrid Density Functionals. *Phys. Chem. Chem. Phys.* **2009**, *11*, 4611−4620.

(16) Brémond, E.; Ciofini, I.; Sancho-García, J. C.; Adamo, C. Nonempirical Double-Hybrid Functionals: An Effective Tool for Chemists. *Acc. Chem. Res.* **2016**, *49*, 1503−1513.

(17) Schwabe, T.; Goerigk, L. Time-Dependent Double-Hybrid Density Functionals with Spin-Component and Spin-Opposite Scaling. *J. Chem. Theory Comput.* **2017**, *13*, 4307−4323.

(18) Mester, D.; Kállay, M. A Simple Range-Separated Double-Hybrid Density Functional Theory for Excited States. *J. Chem. Theory Comput.* **2021**, *17*, 927−942.

(19) Hanke, W.; Sham, L. J. Many-Particle Effects in the Optical Excitations of a Semiconductor. *Phys. Rev. Lett.* **1979**, *43*, No. 387.

(20) Strinati, G. Application of the Green's Functions Method to the Study of the Optical Properties of Semiconductors. *Riv. Nuovo Cimento* **1988**, *11*, 1−86.

(21) Onida, G.; Reining, L.; Rubio, A. Electronic Excitations: Density-Functional Versus Many-Body Green's-Function Approaches. *Rev. Mod. Phys.* **2002**, *74*, No. 601.

(22) Martin, R. M.; Reining, L.; Ceperley, D. M. *Interacting Electrons: Theory and Computational Approaches*; Cambridge University Press: Cambridge, 2016.

(23) Hedin, L. New Method for Calculating the One-Particle Green's Function with Application to the Electron-Gas Problem. *Phys. Rev.* **1965**, *139*, No. A796.

(24) Aryasetiawan, F.; Gunnarsson, O. The GW method. *Rep. Prog. Phys.* **1998**, *61*, No. 237.

(25) Golze, D.; Dvorak, M.; Rinke, P. The *GW* Compendium: A Practical Guide to Theoretical Photoemission Spectroscopy. *Front. Chem.* **2019**, *7*, No. 377.

(26) Marie, A.; Ammar, A.; Loos, P.-F. The *GW* Approximation: A Quantum Chemistry Perspective. In *Advances in Quantum Chemistry*; Elsevier, 2023.

(27) Blase, X.; Duchemin, I.; Jacquemin, D. The Bethe-Salpeter Equation in Chemistry: Relations with TD-DFT, Applications and Challenges. *Chem. Soc. Rev.* **2018**, *47*, 1022−1043.

(28) Gui, X.; Holzer, C.; Klopper, W. Accuracy Assessment of *GW* Starting Points for Calculating Molecular Excitation Energies Using the Bethe-Salpeter Formalism. *J. Chem. Theory Comput.* **2018**, *14*, 2127−2136.

(29) Blase, X.; Duchemin, I.; Jacquemin, D.; Loos, P.-F. The Bethe−Salpeter Equation Formalism: From Physics to Chemistry. *J. Phys. Chem. Lett.* **2020**, *11*, 7371−7382.

(30) Christiansen, O.; Koch, H.; Jørgensen, P. The Second-Order Approximate Coupled Cluster Singles and Doubles Model CC2. *Chem. Phys. Lett.* **1995**, *243*, 409−418.

(31) Hättig, C.; Weigend, F. CC2 Excitation Energy Calculations on Large Molecules Using the Resolution of the Identity Approximation. *J. Chem. Phys.* **2000**, *113*, 5154−5161.
(32) Purvis, G. D., III; Bartlett, R. J. A Full Coupled-Cluster Singles and Doubles Model: The Inclusion of Disconnected Triples. *J. Chem. Phys.* **1982**, *76*, 1910−1918.
(33) Scuseria, G. E.; Scheiner, A. C.; Lee, T. J.; Rice, J. E.; Schaefer, H. F. The Closed-Shell Coupled Cluster Single and Double Excitation (CCSD) Model for the Description of Electron Correlation. A Comparison with Configuration Interaction (CISD) Results. *J. Chem. Phys.* **1987**, *86*, 2881−2890.
(34) Koch, H.; Jensen, H. J. A.; Jorgensen, P.; Helgaker, T. Excitation Energies from the Coupled Cluster Singles and Doubles Linear Response Function (CCSDLR). Applications to Be, CH^+, CO, and H_2O. *J. Chem. Phys.* **1990**, *93*, 3345−3350.
(35) Stanton, J. F.; Bartlett, R. J. The Equation of Motion Coupled-Cluster Method - A Systematic Biorthogonal Approach to Molecular Excitation Energies, Transition-Probabilities, and Excited-State Properties. *J. Chem. Phys.* **1993**, *98*, 7029−7039.
(36) Stanton, J. F. Many-Body Methods for Excited State Potential Energy Surfaces. I: General Theory of Energy Gradients for the Equation-of-Motion Coupled-Cluster Method. *J. Chem. Phys.* **1993**, *99*, 8840−8847.
(37) Christiansen, O.; Koch, H.; Jørgensen, P. Response Functions in the CC3 Iterative Triple Excitation Model. *J. Chem. Phys.* **1995**, *103*, 7429−7441.
(38) Koch, H.; Christiansen, O.; Jorgensen, P.; Olsen, J. Excitation Energies of BH, CH_2 and Ne in Full Configuration Interaction and the Hierarchy CCS, CC2, CCSD and CC3 of Coupled Cluster Models. *Chem. Phys. Lett.* **1995**, *244*, 75−82.
(39) Koch, H.; Christiansen, O.; Jorgensen, P.; de Merás, A. M. S.; Helgaker, T. The CC3 Model: An Iterative Coupled Cluster Approach Including Connected Triples. *J. Chem. Phys.* **1997**, *106*, 1808−1818.
(40) Noga, J.; Bartlett, R. J. The Full CCSDT Model for Molecular Electronic Structure. *J. Chem. Phys.* **1987**, *86*, 7041−7050.
(41) Scuseria, G. E.; Schaefer, H. F. A New Implementation of the Full CCSDT Model for Molecular Electronic Structure. *Chem. Phys. Lett.* **1988**, *152*, 382−386.
(42) Kucharski, S. A.; Włoch, M.; Musiał, M.; Bartlett, R. J. Coupled-Cluster Theory for Excited Electronic States: The Full Equation-Of-Motion Coupled-Cluster Single, Double, and Triple Excitation Method. *J. Chem. Phys.* **2001**, *115*, 8263−8266.
(43) Kowalski, K.; Piecuch, P. The Active-Space Equation-of-Motion Coupled-Cluster Methods for Excited Electronic States: Full EOMCCSDt. *J. Chem. Phys.* **2001**, *115*, 643−651.
(44) Kowalski, K.; Piecuch, P. Excited-State Potential Energy Curves of CH^+: a Comparison of the EOMCCSDt And Full EOMCCSDT Results. *Chem. Phys. Lett.* **2001**, *347*, 237−246.
(45) Kállay, M.; Gauss, J. Calculation of Excited-State Properties Using General Coupled-Cluster and Configuration-Interaction Models. *J. Chem. Phys.* **2004**, *121*, 9257−9269.
(46) Kállay, M.; Gauss, J. Approximate Treatment of Higher Excitations in Coupled-Cluster Theory. *J. Chem. Phys.* **2005**, *123*, No. 214105.
(47) Loos, P.-F.; Matthews, D. A.; Lipparini, F.; Jacquemin, D. How Accurate are EOM-CC4 Vertical Excitation Energies? *J. Chem. Phys.* **2021**, *154*, No. 221103.
(48) Loos, P.-F.; Lipparini, F.; Matthews, D. A.; Blondel, A.; Jacquemin, D. A Mountaineering Strategy to Excited States: Revising Reference Values with EOM-CC4. *J. Chem. Theory Comput.* **2022**, *18*, 4418−4427.
(49) Kucharski, S. A.; Bartlett, R. J. Recursive Intermediate Factorization and Complete Computational Linearization of the Coupled-Cluster Single, Double, Triple, and Quadruple Excitation Equations. *Theor. Chim. Acta* **1991**, *80*, 387−405.
(50) Hirata, S. Higher-Order Equation-of-Motion Coupled-Cluster Methods. *J. Chem. Phys.* **2004**, *121*, 51−59.
(51) Kállay, M.; Gauss, J.; Szalay, P. G. Analytic First Derivatives for General Coupled-Cluster and Configuration Interaction Models. *J. Chem. Phys.* **2003**, *119*, 2991−3004.
(52) Véril, M.; Scemama, A.; Caffarel, M.; Lipparini, F.; Boggio-Pasqua, M.; Jacquemin, D.; Loos, P.-F. QUESTDB: a Database of Highly-Accurate Excitation Energies for the Electronic Structure Community. *WIREs Comput. Mol. Sci.* **2021**, *11*, No. e1517.
(53) Loos, P.-F.; Jacquemin, D. A Mountaineering Strategy to Excited States: Highly Accurate Energies and Benchmarks for Bicyclic Systems. *J. Phys. Chem. A* **2021**, *125*, 10174−10188.
(54) Hohenstein, E. G.; Zhao, Y.; Parrish, R. M.; Martínez, T. J. Rank Reduced Coupled Cluster Theory. II. Equation-of-Motion Coupled-Cluster Singles and Doubles. *J. Chem. Phys.* **2019**, *151*, No. 164121.
(55) Christie, R. M. *Colour Chemistry*; The Royal Society of Chemistry: Cambridge, UK, 1991; p 228.
(56) Zollinger, H. *Color Chemistry, Syntheses, Properties and Applications of Organic Dyes and Pigments*, 3rd ed.; Wiley-VCH: Weinheim, 2003; p 647.
(57) Valeur, B. *Molecular Fluorescence: Principles and Applications*; Wiley-VCH: Weinheim, 2002.
(58) Huron, B.; Malrieu, J. P.; Rancurel, P. Iterative Perturbation Calculations of Ground and Excited State Energies from Multi-configurational Zeroth-Order Wavefunctions. *J. Chem. Phys.* **1973**, *58*, 5745−5759.
(59) Garniron, Y.; Scemama, A.; Giner, E.; Caffarel, M.; Loos, P.-F. Selected Configuration Interaction Dressed by Perturbation. *J. Chem. Phys.* **2018**, *149*, No. 064103.
(60) Garniron, Y.; Applencourt, T.; Gasperich, K.; Benali, A.; Ferté, A.; Paquier, J.; Pradines, B.; Assaraf, R.; Reinhardt, P.; Toulouse, J.; Barbaresco, P.; Renon, N.; David, G.; Malrieu, J.-P.; Véril, M.; Caffarel, M.; Loos, P.-F.; Giner, E.; Scemama, A. Quantum Package 2.0: An Open-Source Determinant-Driven Suite of Programs. *J. Chem. Theory Comput.* **2019**, *15*, 3591−3609.
(61) Eriksen, J. J.; Anderson, T. A.; Deustua, J. E.; Ghanem, K.; Hait, D.; Hoffmann, M. R.; Lee, S.; Levine, D. S.; Magoulas, I.; Shen, J.; Tubman, N. M.; Whaley, K. B.; Xu, E.; Yao, Y.; Zhang, N.; Alavi, A.; Chan, G. K.-L.; Head-Gordon, M.; Liu, W.; Piecuch, P.; Sharma, S.; Ten-no, S. L.; Umrigar, C. J.; Gauss, J. The Ground State Electronic Energy of Benzene. *J. Phys. Chem. Lett.* **2020**, *11*, 8922−8929.
(62) Loos, P.-F.; Damour, Y.; Scemama, A. The performance of CIPSI on the ground state electronic energy of benzene. *J. Chem. Phys.* **2020**, *153*, No. 176101.
(63) Eriksen, J. J. The Shape of Full Configuration Interaction to Come. *J. Phys. Chem. Lett.* **2021**, *12*, 418−432.
(64) Hutcheson, A.; Paul, A. C.; Myhre, R. H.; Koch, H.; Høyvik, I.-M. Describing Ground and Excited State Potential Energy Surfaces for Molecular Photoswitches using Coupled Cluster Models. *J. Comput. Chem.* **2021**, *42*, 1419−1429.
(65) Paul, A. C.; Folkestad, S. D.; Myhre, R. H.; Koch, H. Oscillator Strengths in the Framework of Equation of Motion Multilevel CC3. *J. Chem. Theory Comput.* **2022**, *18*, 5246−5258.
(66) Loos, P.-F.; Lipparini, F.; Jacquemin, D. Heptazine, Cyclazine, and Related Compounds: Chemically-Accurate Estimates of the Inverted Singlet−Triplet Gap. *J. Phys. Chem. Lett.* **2023**, *14*, 11069−11075.
(67) Silva, M. R., Junior; Schreiber, M.; Sauer, S. P. A.; Thiel, W. Benchmarks for Electronically Excited States: Time-Dependent Density Functional Theory and Density Functional Theory Based Multireference Configuration Interaction. *J. Chem. Phys.* **2008**, *129*, No. 104103.
(68) Silva-Junior, M. R.; Sauer, S. P. A.; Schreiber, M.; Thiel, W. Basis Set Effects on Coupled Cluster Benchmarks of Electronically Excited States: CC3, CCSDR(3) and CC2. *Mol. Phys.* **2010**, *108*, 453−465.
(69) Zuev, D.; Bravaya, K. B.; Crawford, T. D.; Lindh, R.; Krylov, A. I. Electronic Structure of the two Isomers of the Anionic Form of *p*-Coumaric Acid Chromophore. *J. Chem. Phys.* **2011**, *134*, No. 034310.

https://doi.org/10.1021/acs.jctc.4c00906
J. Chem. Theory Comput. 2024, 20, 8152−8174

(70) Kánnár, D.; Szalay, P. G. Benchmarking Coupled Cluster Methods on Singlet Excited States of Nucleobases. *J. Mol. Model.* **2014**, *20*, No. 2503.
(71) Cuzzocrea, A.; Moroni, S.; Scemama, A.; Filippi, C. Reference Excitation Energies of Increasingly Large Molecules: A QMC Study of Cyanine Dyes. *J. Chem. Theory Comput.* **2022**, *18*, 1089−1095.
(72) Loos, P.-F.; Comin, M.; Blase, X.; Jacquemin, D. Reference Energies for Intramolecular Charge-Transfer Excitations. *J. Chem. Theory Comput.* **2021**, *17*, 3666−3686.
(73) Frank, M. S.; Schmitz, G.; Hättig, C. Implementation of the Iterative Triples Model CC3 for Excitation Energies using Pair Natural Orbitals and Laplace Transformation Techniques. *J. Chem. Phys.* **2020**, *153*, No. 034109.
(74) Paul, A. C.; Myhre, R. H.; Koch, H. New and Efficient Implementation of CC3. *J. Chem. Theory Comput.* **2021**, *17*, 117−126.
(75) Goerigk, L.; Grimme, S. Assessment of TD-DFT Methods and of Various Spin Scaled CIS$_n$D and CC2 Versions for the Treatment of Low-Lying Valence Excitations of Large Organic Dyes. *J. Chem. Phys.* **2010**, *132*, No. 184103.
(76) Send, R.; Valsson, O.; Filippi, C. Electronic Excitations of Simple Cyanine Dyes: Reconciling Density Functional and Wave Function Methods. *J. Chem. Theory Comput.* **2011**, *7*, 444−455.
(77) Winter, N. O. C.; Graf, N. K.; Leutwyler, S.; Hättig, C. Benchmarks for 0−0 Transitions of Aromatic Organic Molecules: DFT/B3LYP, ADC(2), CC2, SOS-CC2 and SCS-CC2 Compared to High-resolution Gas-Phase Data. *Phys. Chem. Chem. Phys.* **2013**, *15*, 6623−6630.
(78) Jacquemin, D.; Duchemin, I.; Blase, X. 0−0 Energies Using Hybrid Schemes: Benchmarks of TD-DFT, CIS(D), ADC(2), CC2, and BSE/GW formalisms for 80 Real-Life Compounds. *J. Chem. Theory Comput.* **2015**, *11*, 5340−5359.
(79) Oruganti, B.; Fang, C.; Durbeej, B. Assessment of a Composite CC2/DFT Procedure for Calculating 0−0 Excitation Energies of Organic Molecules. *Mol. Phys.* **2016**, *114*, 3448−3463.
(80) Auer, A. A.; Bartlett, R. J.; Benedikt, U.; Berger, C.; Bernholdt, D. E.; Bomble, Y. J.; Christiansen, O.; Engel, F.; Faber, R.; Heckert, M.; Heun, O.; Hilgenberg, M.; Huber, C.; Jagau, T.-C.; Jonsson, D.; Jusélius, J.; Kirsch, T.; Klein, K.; Lauderdale, W. J.; Lipparini, F.; Metzroth, T.; Mück, L. A.; O'Neill, D. P.; Price, D. R.; Prochnow, E.; Puzzarini, C.; Ruud, K.; Schiffmann, F.; Schwalbach, W.; Simmons, C.; Stopkowicz, S.; Tajti, A.; Vázquez, J.; Wang, F.; Watts, J. D.et al. CFOUR, Coupled-Cluster Techniques for Computational Chemistry, a Quantum-Chemical Program Package. http://www.cfour.de.
(81) Matthews, D. A.; Cheng, L.; Harding, M. E.; Lipparini, F.; Stopkowicz, S.; Jagau, T.-C.; Szalay, P. G.; Gauss, J.; Stanton, J. F. Coupled-Cluster Techniques for Computational Chemistry: The CFOUR Program Package. *J. Chem. Phys.* **2020**, *152*, No. 214108.
(82) Frisch, M. J.; Trucks, G. W.; Schlegel, H. B.; Scuseria, G. E.; Robb, M. A.; Cheeseman, J. R.; Scalmani, G.; Barone, V.; Petersson, G. A.; Nakatsuji, H.; Li, X.; Caricato, M.; Marenich, A. V.; Bloino, J.; Janesko, B. G.; Gomperts, R.; Mennucci, B.; Hratchian, H. P.; Ortiz, J. V.; Izmaylov, A. F.; Sonnenberg, J. L.; Williams-Young, D.; Ding, F.; Lipparini, F.; Egidi, F.; Goings, J.; Peng, B.; Petrone, A.; Henderson, T.; Ranasinghe, D.; Zakrzewski, V. G.; Gao, J.; Rega, N.; Zheng, G.; Liang, W.; Hada, M.; Ehara, M.; Toyota, K.; Fukuda, R.; Hasegawa, J.; Ishida, M.; Nakajima, T.; Honda, Y.; Kitao, O.; Nakai, H.; Vreven, T.; Throssell, K.; Montgomery, J. A., Jr.; Peralta, J. E.; Ogliaro, F.; Bearpark, M. J.; Heyd, J. J.; Brothers, E. N.; Kudin, K. N.; Staroverov, V. N.; Keith, T. A.; Kobayashi, R.; Normand, J.; Raghavachari, K.; Rendell, A. P.; Burant, J. C.; Iyengar, S. S.; Tomasi, J.; Cossi, M.; Millam, J. M.; Klene, M.; Adamo, C.; Cammi, R.; Ochterski, J. W.; Martin, R. L.; Morokuma, K.; Farkas, O.; Foresman, J. B.; Fox, D. J. *Gaussian 16*, Revision A.03; Gaussian Inc.: Wallingford CT, 2016.
(83) Aidas, K.; Angeli, C.; Bak, K. L.; Bakken, V.; Bast, R.; Boman, L.; Christiansen, O.; Cimiraglia, R.; Coriani, S.; Dahle, P.; Dalskov, E. K.; Ekström, U.; Enevoldsen, T.; Eriksen, J. J.; Ettenhuber, P.; Fernández, B.; Ferrighi, L.; Fliegl, H.; Frediani, L.; Hald, K.; Halkier, A.; Hättig, C.; Heiberg, H.; Helgaker, T.; Hennum, A. C.; Hettema, H.; Hjertenæs, E.; Høst, S.; Hoyvik, I.-M.; Iozzi, M. F.; Jansik, B.; Jensen, H. J. A.; Jonsson, D.; Jørgensen, P.; Kauczor, J.; Kirpekar, S.; Kjærgaard, T.; Klopper, W.; Knecht, S.; Kobayashi, R.; Koch, H.; Kongsted, J.; Krapp, A.; Kristensen, K.; Ligabue, A.; Lutnæs, O. B.; Melo, J. I.; Mikkelsen, K. V.; Myhre, R. H.; Neiss, C.; Nielsen, C. B.; Norman, P.; Olsen, J.; Olsen, J. M. H.; Osted, A.; Packer, M. J.; Pawlowski, F.; Pedersen, T. B.; Provasi, P. F.; Reine, S.; Rinkevicius, Z.; Ruden, T. A.; Ruud, K.; Rybkin, V. V.; Sałek, P.; Samson, C. C. M.; de Merás, A. S.; Saue, T.; Sauer, S. P. A.; Schimmelpfennig, B.; Sneskov, K.; Steindal, A. H.; Sylvester-Hvid, K. O.; Taylor, P. R.; Teale, A. M.; Tellgren, E. I.; Tew, D. P.; Thorvaldsen, A. J.; Thogersen, L.; Vahtras, O.; Watson, M. A.; Wilson, D. J. D.; Ziolkowski, M.; Ågren, H. The Dalton Quantum Chemistry Program System. *WIREs Comput. Mol. Sci.* **2014**, *4*, 269−284.
(84) Balabanov, N. B.; Peterson, K. A. Basis set Limit Electronic Excitation Energies, Ionization Potentials, and Electron Affinities for the 3*d* Transition Metal Atoms: Coupled Cluster and Multireference Methods. *J. Chem. Phys.* **2006**, *125*, No. 074110.
(85) Kamiya, M.; Hirata, S. Higher-Order Equation-of-Motion Coupled-Cluster Methods for Ionization Processes. *J. Chem. Phys.* **2006**, *125*, No. 074111.
(86) Peach, M. J. G.; Tozer, D. J. Overcoming Low Orbital Overlap and Triplet Instability Problems in TDDFT. *J. Phys. Chem. A* **2012**, *116*, 9783−9789.
(87) Watson, M. A.; Chan, G. K.-L. Excited States of Butadiene to Chemical Accuracy: Reconciling Theory and Experiment. *J. Chem. Theory Comput.* **2012**, *8*, 4013−4018.
(88) Feller, D.; Peterson, K. A.; Davidson, E. R. A Systematic Approach to Vertically Excited States of Ethylene Using Configuration Interaction and Coupled Cluster Techniques. *J. Chem. Phys.* **2014**, *141*, No. 104302.
(89) Franke, P. R.; Moore, K. B.; Schaefer, H. F.; Douberly, G. E. tert-Butyl Peroxy Radical: Ground and First Excited State Energetics and Fundamental Frequencies. *Phys. Chem. Chem. Phys.* **2019**, *21*, 9747−9758.
(90) Casanova-Páez, M.; Dardis, M. B.; Goerigk, L. ωB2PLYP and ωB2GPPLYP: The First Two Double-Hybrid Density Functionals with Long-Range Correction Optimized for Excitation Energies. *J. Chem. Theory Comput.* **2019**, *15*, 4735−4744.
(91) Chrayteh, A.; Blondel, A.; Loos, P.-F.; Jacquemin, D. A Mountaineering Strategy to Excited States: Highly-Accurate Oscillator Strengths and Dipole Moments of Small Molecules. *J. Chem. Theory Comput.* **2021**, *17*, 416−438.
(92) Epifanovsky, E.; Gilbert, A. T. B.; Feng, X.; Lee, J.; Mao, Y.; Mardirossian, N.; Pokhilko, P.; White, A. F.; Coons, M. P.; Dempwolff, A. L.; Gan, Z.; Hait, D.; Horn, P. R.; Jacobson, L. D.; Kaliman, I.; Kussmann, J.; Lange, A. W.; Lao, K. U.; Levine, D. S.; Liu, J.; McKenzie, S. C.; Morrison, A. F.; Nanda, K. D.; Plasser, F.; Rehn, D. R.; Vidal, M. L.; You, Z.-Q.; Zhu, Y.; Alam, B.; Albrecht, B. J.; Aldossary, A.; Alguire, E.; Andersen, J. H.; Athavale, V.; Barton, D.; Begam, K.; Behn, A.; Bellonzi, N.; Bernard, Y. A.; Berquist, E. J.; Burton, H. G. A.; Carreras, A.; Carter-Fenk, K.; Chakraborty, R.; Chien, A. D.; Closser, K. D.; Cofer-Shabica, V.; Dasgupta, S.; de Wergifosse, M.; Deng, J.; Diedenhofen, M.; Do, H.; Ehlert, S.; Fang, P.-T.; Fatehi, S.; Feng, Q.; Friedhoff, T.; Gayvert, J.; Ge, Q.; Gidofalvi, G.; Goldey, M.; Gomes, J.; González-Espinoza, C. E.; Gulania, S.; Gunina, A. O.; Hanson-Heine, M. W. D.; Harbach, P. H. P.; Hauser, A.; Herbst, M. F.; Hernández Vera, M.; Hodecker, M.; Holden, Z. C.; Houck, S.; Huang, X.; Hui, K.; Huynh, B. C.; Ivanov, M.; Jász, Á.; Ji, H.; Jiang, H.; Kaduk, B.; Kähler, S.; Khistyaev, K.; Kim, J.; Kis, G.; Klunzinger, P.; Koczor-Benda, Z.; Koh, J. H.; Kosenkov, D.; Koulias, L.; Kowalczyk, T.; Krauter, C. M.; Kue, K.; Kunitsa, A.; Kus, T.; Ladjánszki, I.; Landau, A.; Lawler, K. V.; Lefrancois, D.; Lehtola, S.; Li, R. R.; Li, Y.-P.; Liang, J.; Liebenthal, M.; Lin, H.-H.; Lin, Y.-S.; Liu, F.; Liu, K.-Y.; Loipersberger, M.; Luenser, A.; Manjanath, A.; Manohar, P.; Mansoor, E.; Manzer, S. F.; Mao, S.-P.; Marenich, A. V.; Markovich, T.; Mason, S.; Maurer, S. A.; McLaughlin, P. F.; Menger, M. F. S. J.; Mewes, J.-M.; Mewes, S. A.; Morgante, P.; Mullinax, J. W.; Oosterbaan, K. J.; Paran, G.; Paul, A. C.; Paul, S. K.; Pavošević, F.; Pei, Z.; Prager, S.; Proynov, E. I.; Rák, Á.; Ramos-

https://doi.org/10.1021/acs.jctc.4c00906
J. Chem. Theory Comput. 2024, 20, 8152−8174

Cordoba, E.; Rana, B.; Rask, A. E.; Rettig, A.; Richard, R. M.; Rob, F.; Rossomme, E.; Scheele, T.; Scheurer, M.; Schneider, M.; Sergueev, N.; Sharada, S. M.; Skomorowski, W.; Small, D. W.; Stein, C. J.; Su, Y.-C.; Sundstrom, E. J.; Tao, Z.; Thirman, J.; Tornai, G. J.; Tsuchimochi, T.; Tubman, N. M.; Veccham, S. P.; Vydrov, O.; Wenzel, J.; Witte, J.; Yamada, A.; Yao, K.; Yeganeh, S.; Yost, S. R.; Zech, A.; Zhang, I. Y.; Zhang, X.; Zhang, Y.; Zuev, D.; Aspuru-Guzik, A.; Bell, A. T.; Besley, N. A.; Bravaya, K. B.; Brooks, B. R.; Casanova, D.; Chai, J.-D.; Coriani, S.; Cramer, C. J.; Cserey, G.; DePrince, A. E.; DiStasio, R. A.; Dreuw, A.; Dunietz, B. D.; Furlani, T. R.; Goddard, W. A.; Hammes-Schiffer, S.; Head-Gordon, T.; Hehre, W. J.; Hsu, C.-P.; Jagau, T.-C.; Jung, Y.; Klamt, A.; Kong, J.; Lambrecht, D. S.; Liang, W.; Mayhall, N. J.; McCurdy, C. W.; Neaton, J. B.; Ochsenfeld, C.; Parkhill, J. A.; Peverati, R.; Rassolov, V. A.; Shao, Y.; Slipchenko, L. V.; Stauch, T.; Steele, R. P.; Subotnik, J. E.; Thom, A. J. W.; Tkatchenko, A.; Truhlar, D. G.; Van Voorhis, T.; Wesolowski, T. A.; Whaley, K. B.; Woodcock, H. L.; Zimmerman, P. M.; Faraji, S.; Gill, P. M. W.; Head-Gordon, M.; Herbert, J. M.; Krylov, A. I. Software for the Frontiers of Quantum Chemistry: An Overview of Developments in the Q-Chem 5 Package. *J. Chem. Phys.* **2021**, *155*, No. 084801.

(93) TURBOMOLE GmbH *TURBOMOLE V7.3*; University of Karlsruhe and Forschungszentrum Karlsruhe GmbH, 2018.

(94) Balasubramani, S. G.; Chen, G. P.; Coriani, S.; Diedenhofen, M.; Frank, M. S.; Franzke, Y. J.; Furche, F.; Grotjahn, R.; Harding, M. E.; Hättig, C.; Hellweg, A.; Helmich-Paris, B.; Holzer, C.; Huniar, U.; Kaupp, M.; Marefat Khah, A.; Karbalaei Khani, S.; Müller, T.; Mack, F.; Nguyen, B. D.; Parker, S. M.; Perlt, E.; Rappoport, D.; Reiter, K.; Roy, S.; Rückert, M.; Schmitz, G.; Sierka, M.; Tapavicza, E.; Tew, D. P.; van Wüllen, C.; Voora, V. K.; Weigend, F.; Wodyński, A.; Yu, J. M. TURBOMOLE: Modular Program Suite for ab initio Quantum-Chemical and Condensed-Matter Simulations. *J. Chem. Phys.* **2020**, *152*, No. 184107.

(95) Head-Gordon, M.; Rico, R. J.; Oumi, M.; Lee, T. J. A Doubles Correction to Electronic Excited States From Configuration Interaction in the Space of Single Substitutions. *Chem. Phys. Lett.* **1994**, *219*, 21−29.

(96) Head-Gordon, M.; Maurice, D.; Oumi, M. A Perturbative Correction to Restricted Open-Shell Configuration-Interaction with Single Substitutions for Excited-States of Radicals. *Chem. Phys. Lett.* **1995**, *246*, 114−121.

(97) Hellweg, A.; Grün, S. A.; Hättig, C. Benchmarking the Performance of Spin-Component Scaled CC2 in Ground and Electronically Excited States. *Phys. Chem. Chem. Phys.* **2008**, *10*, 4119−4127.

(98) Stanton, J. F.; Gauss, J. Perturbative Treatment of the Similarity Transformed Hamiltonian in Equation-of-Motion Coupled-Cluster Approximations. *J. Chem. Phys.* **1995**, *103*, 1064−1076.

(99) Trofimov, A.; Schirmer, J. Polarization Propagator Study of Electronic Excitation in key Heterocyclic Molecules I. Pyrrole. *Chem. Phys.* **1997**, *214*, 153−170.

(100) Dreuw, A.; Wormit, M. The Algebraic Diagrammatic Construction Scheme for the Polarization Propagator for the Calculation of Excited States. *WIREs Comput. Mol. Sci.* **2015**, *5*, 82−95.

(101) Krauter, C. M.; Pernpointner, M.; Dreuw, A. Application of the Scaled-Opposite-Spin Approximation to Algebraic Diagrammatic Construction Schemes of Second Order. *J. Chem. Phys.* **2013**, *138*, No. 044107.

(102) Trofimov, A. B.; Stelter, G.; Schirmer, J. Electron Excitation Energies Using a Consistent Third-Order Propagator Approach: Comparison with Full Configuration Interaction and Coupled Cluster Results. *J. Chem. Phys.* **2002**, *117*, 6402−6410.

(103) Harbach, P. H. P.; Wormit, M.; Dreuw, A. The Third-Order Algebraic Diagrammatic Construction Method (ADC(3)) for the Polarization Propagator for Closed-Shell Molecules: Efficient Implementation and Benchmarking. *J. Chem. Phys.* **2014**, *141*, No. 064113.

(104) Loos, P.-F.; Jacquemin, D. Is ADC(3) as Accurate as CC3 for Valence and Rydberg Transition Energies? *J. Phys. Chem. Lett.* **2020**, *11*, 974−980.

(105) Bauer, M.; Dempwolff, A. L.; Rehn, D. R.; Dreuw, A. Exploring the Accuracy and Usefulness of Semi-Empirically Scaled ADC Schemes by Blending Second and Third Order Terms. *J. Chem. Phys.* **2022**, *156*, No. 144101.

(106) Christiansen, O.; Koch, H.; Jørgensen, P. Perturbative Triple Excitation Corrections to Coupled Cluster Singles and Doubles Excitation Energies. *J. Chem. Phys.* **1996**, *105*, 1451−1459.

(107) Matthews, D. A.; Stanton, J. F. A new Approach to Approximate Equation-Of-Motion Coupled Cluster with Triple Excitations. *J. Chem. Phys.* **2016**, *145*, No. 124102.

(108) Watts, J. D.; Bartlett, R. J. Iterative and Non-Iterative Triple Excitation Corrections in Coupled-Cluster Methods for Excited Electronic States: the EOM-CCSDT-3 and EOM-CCSD($\tilde{T}$) Methods. *Chem. Phys. Lett.* **1996**, *258*, 581−588.

(109) Prochnow, E.; Harding, M. E.; Gauss, J. Parallel Calculation of CCSDT and Mk-MRCCSDT Energies. *J. Chem. Theory Comput.* **2010**, *6*, 2339−2347.

(110) Staroverov, V. N.; Scuseria, G. E.; Tao, J.; Perdew, J. P. Comparative Assessment of a New Nonempirical Density Functional: Molecules and Hydrogen-Bonded Complexes. *J. Chem. Phys.* **2003**, *119*, 12129−12137.

(111) Boese, A. D.; Handy, N. C. New Exchange-Correlation Density Functionals: The Role of the Kinetic-Energy Density. *J. Chem. Phys.* **2002**, *116*, 9559−9569.

(112) Becke, A. D. Density-Functional Thermochemistry. 3. The Role of Exact Exchange. *J. Chem. Phys.* **1993**, *98*, 5648−5652.

(113) Stephens, P. J.; Devlin, F. J.; Chabalowski, C. F.; Frisch, M. J. Ab Initio Calculation of Vibrational Absorption and Circular Dichroism Spectra Using Density Functional Force Fields. *J. Phys. Chem. A* **1994**, *98*, 11623−11627.

(114) Barone, V.; Orlandini, L.; Adamo, C. Proton Transfer in Model Hydrogen-Bonded Systems by a Density Functional Approach. *Chem. Phys. Lett.* **1994**, *231*, 295−300.

(115) Stephens, P. J.; Devlin, F. J.; Frisch, M. J.; Chabalowski, C. F. Ab initio Calculation of Vibrational Absorption and Circular Dichroism Spectra Using Density Functional Force Fields. *J. Phys. Chem. A* **1994**, *98*, 11623−11627.

(116) Adamo, C.; Barone, V. Toward Reliable Density Functional Methods Without Adjustable Parameters: the PBE0 Model. *J. Chem. Phys.* **1999**, *110*, 6158−6170.

(117) Ernzerhof, M.; Scuseria, G. E. Assessment of the Perdew−Burke−Ernzerhof Exchange-Correlation Functional. *J. Chem. Phys.* **1999**, *110*, 5029−5036.

(118) Hui, K.; Chai, J.-D. SCAN-Based Hybrid and Double-Hybrid Density Functionals from Models Without Fitted Parameters. *J. Chem. Phys.* **2016**, *144*, No. 044114.

(119) Zhao, Y.; Truhlar, D. G. The M06 Suite of Density Functionals for Main Group Thermochemistry, Thermochemical Kinetics, Noncovalent Interactions, Excited States, and Transition Elements: Two New Functionals and Systematic Testing of Four M06-Class Functionals and 12 Other Functionals. *Theor. Chem. Acc.* **2008**, *120*, 215−241.

(120) Peverati, R.; Truhlar, D. A Global Hybrid Generalized Gradient Approximation to the Exchange-Correlation Functional That Satisfies the Second-Order Density-Gradient Constraint and Has Broad Applicability in Chemistry. *J. Chem. Phys.* **2011**, *135*, No. 191102.

(121) Boese, A. D.; Martin, J. M. L. Development of Density Functionals for Thermochemical Kinetics. *J. Chem. Phys.* **2004**, *121*, 3405−3416.

(122) Yu, H. S.; He, X.; Li, S. L.; Truhlar, D. G. MN15: A Kohn-Sham Global-Hybrid Exchange-Correlation Density Functional with Broad Accuracy for Multi-Reference and Single-Reference Systems and Noncovalent Interactions. *Chem. Sci.* **2016**, *7*, 5032−5051.

(123) Zhao, Y.; Truhlar, D. G. Exploring the Limit of Accuracy of the Global Hybrid Meta Density Functional for Main-Group

https://doi.org/10.1021/acs.jctc.4c00906
J. Chem. Theory Comput. 2024, 20, 8152−8174

Thermochemistry, Kinetics, and Noncovalent Interactions. *J. Chem. Theory Comput.* **2008**, *4*, 1849−1868.
(124) Wang, Y.; Verma, P.; Zhang, L.; Li, Y.; Liu, Z.; Truhlar, D. G.; He, X. M06-SX Screened-Exchange Density Functional for Chemistry and Solid-State Physics. *Proc. Natl. Acad. Sci. U.S.A.* **2020**, *117*, 2294−2301.
(125) Yanai, T.; Tew, D. P.; Handy, N. C. A New Hybrid Exchange-Correlation Functional Using the Coulomb-Attenuating Method (CAM-B3LYP). *Chem. Phys. Lett.* **2004**, *393*, 51−56.
(126) Okuno, K.; Shigeta, Y.; Kishi, R.; Miyasaka, H.; Nakano, M. Tuned CAM-B3LYP Functional in the Time-Dependent Density Functional Theory Scheme for Excitation Energies and Properties of Diarylethene Derivatives. *J. Photochem. Photobiol., A* **2012**, *235*, 29−34.
(127) Day, P. N.; Nguyen, K. A.; Pachter, R. Calculation of Two-Photon Absorption Spectra of Donor-π-Acceptor Compounds in Solution using Quadratic Response Time-Dependent Density Functional Theory. *J. Chem. Phys.* **2006**, *125*, No. 094103.
(128) Cohen, A. J.; Mori-Sánchez, P.; Yang, W. Development of Exchange-Correlation Functionals with Minimal Many-Electron Self-Interaction Error. *J. Chem. Phys.* **2007**, *126*, No. 191109.
(129) Chai, J. D.; Head-Gordon, M. Long-range Corrected Hybrid Density Functionals with Damped Atom−Atom Dispersion Corrections. *Phys. Chem. Chem. Phys.* **2008**, *10*, 6615−6620.
(130) Mardirossian, N.; Head-Gordon, M. ωB97M-V: A Combinatorially Optimized, Range-Separated Hybrid, meta-GGA Density Functional with VV10 Nonlocal Correlation. *J. Chem. Phys.* **2016**, *144*, No. 214110.
(131) Chai, J. D.; Head-Gordon, M. Systematic Optimization of Long-Range Corrected Hybrid Density Functionals. *J. Chem. Phys.* **2008**, *128*, No. 084106.
(132) Henderson, T. M.; Izmaylov, A. F.; Scalmani, G.; Scuseria, G. E. Can Short-Range Hybrids Describe Long-Range-Dependent Properties? *J. Chem. Phys.* **2009**, *131*, No. 044108.
(133) Peverati, R.; Truhlar, D. Improving the Accuracy of Hybrid Meta-GGA Density Functionals by Range Separation. *J. Phys. Chem. Lett.* **2011**, *2*, 2810−2817.
(134) We used xc_grid/3, cis_convergence/7, scf_convergence/9, thresh/14, and s2thresh/16.
(135) Bates, J. E. E.; Furche, F. Harnessing the meta-Generalized Gradient Approximation for Time-Dependent Density Functional Theory. *J. Chem. Phys.* **2012**, *137*, No. 164105.
(136) Grotjahn, R.; Furche, F.; Kaupp, M. Importance of Imposing Gauge Invariance in Time-Dependent Density Functional Theory Calculations with meta-Generalized Gradient Approximations. *J. Chem. Phys.* **2022**, *157*, No. 111102.
(137) Liang, J.; Feng, X.; Hait, D.; Head-Gordon, M. Revisiting the Performance of Time-Dependent Density Functional Theory for Electronic Excitations: Assessment of 43 Popular and Recently Developed Functionals from Rungs One to Four. *J. Chem. Theory Comput.* **2022**, *18*, 3460−3473.
(138) Grotjahn, R.; Furche, F. Gauge-Invariant Excited-State Linear and Quadratic Response Properties within the meta-Generalized Gradient Approximation. *J. Chem. Theory Comput.* **2023**, *19*, 4897−4911.
(139) Neese, F.; Wennmohs, F.; Becker, U.; Riplinger, C. The ORCA Quantum Chemistry Program Package. *J. Chem. Phys.* **2020**, *152*, No. 224108.
(140) Grimme, S. Semiempirical Hybrid Density Functional with Perturbative Second-Order Correlation. *J. Chem. Phys.* **2006**, *124*, No. 034108.
(141) Brémond, E.; Adamo, C. Seeking for parameter-free double-hybrid functionals: The PBE0-DH model. *J. Chem. Phys.* **2011**, *135*, No. 024106.
(142) Brémond, É.; Sancho-García, J. C.; Pérez-Jiménez, Á. J.; Adamo, C. Double-hybrid functionals from adiabatic-connection: The QIDH model. *J. Chem. Phys.* **2014**, *141*, No. 031101.
(143) Brémond, É.; Pérez-Jiménez, Á. J.; Sancho-García, J. C.; Adamo, C. Range-Separated Hybrid Density Functionals Made Simple. *J. Chem. Phys.* **2019**, *150*, No. 201102.
(144) Brémond, É.; Savarese, M.; Pérez-Jiménez, Á. J.; Sancho-García, J. C.; Adamo, C. Range-Separated Double-Hybrid Functional from Nonempirical Constraints. *J. Chem. Theory Comput.* **2018**, *14*, 4052−4062.
(145) Chai, J.-D.; Head-Gordon, M. Long-Range Corrected Double-Hybrid Density Functionals. *J. Chem. Phys.* **2009**, *131*, No. 174105.
(146) Casanova-Páez, M.; Goerigk, L. Time-Dependent Long-Range-Corrected Double-Hybrid Density Functionals with Spin-Component and Spin-Opposite Scaling: A Comprehensive Analysis of Singlet−Singlet and Singlet−Triplet Excitation Energies. *J. Chem. Theory Comput.* **2021**, *17*, 5165−5186.
(147) Arbuznikov, A. V.; Kaupp, M. Importance of the Correlation Contribution for Local Hybrid Functionals: Range Separation Aad Self-Interaction Corrections. *J. Chem. Phys.* **2012**, *136*, No. 014111.
(148) Arbuznikov, A. V.; Kaupp, M. Towards Improved Local Hybrid Functionals by Calibration of Exchange-Energy Densities. *J. Chem. Phys.* **2014**, *141*, No. 204101.
(149) Haasler, M.; Maier, T. M.; Grotjahn, R.; Gückel, S.; Arbuznikov, A. V.; Kaupp, M. A Local Hybrid Functional with Wide Applicability and Good Balance between (De)Localization and Left−Right Correlation. *J. Chem. Theory Comput.* **2020**, *16*, 5645−5657.
(150) Sears, J. S.; Koerzdoerfer, T.; Zhang, C. R.; Brédas, J. L. Orbital Instabilities and Triplet States From Time-Dependent Density Functional Theory and Long-Range Corrected Functionals. *J. Chem. Phys.* **2011**, *135*, No. 151103.
(151) Peach, M. J. G.; Williamson, M. J.; Tozer, D. J. Influence of Triplet Instabilities in TDDFT. *J. Chem. Theory Comput.* **2011**, *7*, 3578−3585.
(152) Peach, M. J. G.; Warner, N.; Tozer, D. J. On the Triplet Instability in TDDFT. *Mol. Phys.* **2013**, *111*, 1271−1274.
(153) Rangel, T.; Hamed, S. M.; Bruneval, F.; Neaton, J. B. Evaluating the *GW* Approximation with CCSD(T) for Charged Excitations Across the Oligoacenes. *J. Chem. Theory Comput.* **2016**, *12*, 2834−2842.
(154) Kaplan, F.; Harding, M. E.; Seiler, C.; Weigend, F.; Evers, F.; van Setten, M. J. Quasi-Particle Self-Consistent *GW* for Molecules. *J. Chem. Theory Comput.* **2016**, *12*, 2528−2541.
(155) Duchemin, I.; Blase, X. Robust Analytic-Continuation Approach to Many-Body GW Calculations. *J. Chem. Theory Comput.* **2020**, *16*, 1742−1756.
(156) Duchemin, I.; Blase, X. Cubic-Scaling All-Electron *GW* Calculations with a Separable Density-Fitting Space−Time Approach. *J. Chem. Theory Comput.* **2021**, *17*, 2383−2393.
(157) Ren, X.; Rinke, P.; Blum, V.; Wieferink, J.; Tkatchenko, A.; Sanfilippo, A.; Reuter, K.; Scheffler, M. Resolution-of-Identity Approach to Hartree-Fock, Hybrid Density Functionals, RPA, MP2 and GW with Numeric Atom-Centered Orbital Basis Functions. *New J. Phys.* **2012**, *14*, No. 053020.
(158) Loos, P.-F.; Boggio-Pasqua, M.; Scemama, A.; Caffarel, M.; Jacquemin, D. Reference Energies for Double Excitations. *J. Chem. Theory Comput.* **2019**, *15*, 1939−1956.
(159) Kossoski, F.; Boggio-Pasqua, M.; Loos, P.-F.; Jacquemin, D. Reference Energies for Double Excitations: Improvement and Extension. *J. Chem. Theory Comput.* **2024**, *20*, 5655−5678.
(160) Schreiber, M.; Silva, M. R., Junior; Sauer, S. P. A.; Thiel, W. Benchmarks for Electronically Excited States: CASPT2, CC2, CCSD and CC3. *J. Chem. Phys.* **2008**, *128*, No. 134110.
(161) Sarkar, R.; Loos, P.-F.; Boggio-Pasqua, M.; Jacquemin, D. Assessing the Performances of CASPT2 and NEVPT2 for Vertical Excitation Energies. *J. Chem. Theory Comput.* **2022**, *18*, 2418−2436.
(162) Boggio-Pasqua, M.; Jacquemin, D.; Loos, P.-F. Benchmarking CASPT3 vertical excitation energies. *J. Chem. Phys.* **2022**, *157*, No. 014103.
(163) Loos, P.-F.; Jacquemin, D. A Mountaineering Strategy to Excited States: Accurate Vertical Transition Energies and Benchmarks

https://doi.org/10.1021/acs.jctc.4c00906
J. Chem. Theory Comput. 2024, 20, 8152−8174

for Substituted Benzenes. *J. Comput. Chem.* **2024**, *45*, 1791−1805, DOI: 10.1002/jcc.27358.
(164) Kurashige, Y.; Yanai, T. Theoretical Study of the $\pi \rightarrow \pi^*$ Excited States of Oligoacenes: A Full π-Valence DMRG-CASPT2 Study. *Bull. Chem. Soc. Jpn.* **2014**, *87*, 1071−1073.
(165) Bettanin, F.; Ferrão, L. F. A.; Pinheiro, M. J.; Aquino, A. J. A.; Lischka, H.; Machado, F. B. C.; Nachtigallova, D. Singlet L_a and L_b Bands for *N*-Acenes (N = 2−7): A CASSCF/CASPT2 Study. *J. Chem. Theory Comput.* **2017**, *13*, 4297−4306.
(166) Schriber, J. B.; Hannon, K. P.; Li, C.; Evangelista, F. A. A Combined Selected Configuration Interaction and Many-Body Treatment of Static and Dynamical Correlation in Oligoacenes. *J. Chem. Theory Comput.* **2018**, *14*, 6295−6305.
(167) Sharma, P.; Bernales, V.; Knecht, S.; Truhlar, D. G.; Gagliardi, L. Density Matrix Renormalization Group Pair-Density Functional Theory (Dmrg-Pdft): Singlet−Triplet Gaps in Polyacenes and Polyacetylenes. *Chem. Sci.* **2019**, *10*, 1716−1723.
(168) Momeni, M. R.; Brown, A. Why Do TD-DFT Excitation Energies of BODIPY/Aza-BODIPY Families Largely Deviate from Experiment? Answers from Electron Correlated and Multireference Methods. *J. Chem. Theory Comput.* **2015**, *11*, 2619−2632.
(169) Casellas, J.; Bearpark, M. J.; Reguero, M. Excited-State Decay in the Photoisomerisation of Azobenzene: A New Balance between Mechanisms. *ChemPhysChem* **2016**, *17*, 3068−3079.
(170) Aleotti, F.; Soprani, L.; Nenov, A.; Berardi, R.; Arcioni, A.; Zannoni, C.; Garavelli, M. Multidimensional Potential Energy Surfaces Resolved at the RASPT2 Level for Accurate Photoinduced Isomerization Dynamics of Azobenzene. *J. Chem. Theory Comput.* **2019**, *15*, 6813−6823.
(171) De Vetta, M.; González, L.; Corral, I. The Role of Electronic Triplet States and High-Lying Singlet States in the Deactivation Mechanism of the Parent BODIPY: An ADC(2) and CASPT2 Study. *ChemPhotoChem* **2019**, *3*, 727−738.
(172) Briggs, E. A.; Besley, N. A.; Robinson, D. QM/MM Excited State Molecular Dynamics and Fluorescence Spectroscopy of BODIPY. *J. Phys. Chem. A* **2013**, *117*, 2644−2650.
(173) Gan, Y.; Yue, L.; Guo, X.; Zhu, C.; Cao, Z. Multi-State Nonadiabatic Deactivation Mechanism of Coumarin Revealed by ab initio on-the-fly Trajectory Surface Hopping Dynamic Simulation. *Phys. Chem. Chem. Phys.* **2017**, *19*, 12094−12106.
(174) Ricci, G.; San-Fabián, E.; Olivier, Y.; Sancho-García, J. C. Singlet-Triplet Excited-State Inversion in Heptazine and Related Molecules: Assessment of TD-DFT and ab initio Methods. *ChemPhysChem* **2021**, *22*, 553−560.
(175) Ghosh, S.; Bhattacharyya, K. Origin of the Failure of Density Functional Theories in Predicting Inverted Singlet-Triplet Gaps. *J. Phys. Chem. A* **2022**, *126*, 1378−1385.
(176) Tučková, L.; Straka, M.; Valiev, R. R.; Sundholm, D. On the Origin of the Inverted Singlet-Triplet Gap of the 5th Generation Light-Emitting Molecules. *Phys. Chem. Chem. Phys.* **2022**, *24*, 18713−18721.
(177) Drwal, D.; Matousek, M.; Golub, P.; Tucholska, A.; Hapka, M.; Brabec, J.; Veis, L.; Pernal, K. The Role of Spin Polarization and Dynamic Correlation in Singlet-Triplet Gap Inversion of Heptazine Derivatives. *J. Chem. Theory Comput.* **2023**, *19*, 7606−7616.
(178) Robertson, C.; Worth, G. Modelling the Non-Radiative Singlet Excited State Isomerization of Diphenyl-Acetylene: A Vibronic Coupling Model. *Chem. Phys.* **2018**, *510*, 17−29.
(179) Loos, P.-F.; Scemama, A.; Blondel, A.; Garniron, Y.; Caffarel, M.; Jacquemin, D. A Mountaineering Strategy to Excited States: Highly-Accurate Reference Energies and Benchmarks. *J. Chem. Theory Comput.* **2018**, *14*, 4360−4379.
(180) Loos, P.-F.; Lipparini, F.; Boggio-Pasqua, M.; Scemama, A.; Jacquemin, D. A Mountaineering Strategy to Excited States: Highly-Accurate Energies and Benchmarks for Medium Size Molecules. *J. Chem. Theory Comput.* **2020**, *16*, 1711−1741.
(181) Hättig, C. Response Theory and Molecular Properties (A Tribute to Jan Linderberg and Poul Jørgensen). In *Advances in Quantum Chemistry*; Jensen, H. A., Ed.; Academic Press: Amsterdam, Boston, Heidelberg, 2005; Vol. *50*, pp 37−60.
(182) Kánnár, D.; Tajti, A.; Szalay, P. G. Accuracy of Coupled Cluster Excitation Energies in Diffuse Basis Sets. *J. Chem. Theory Comput.* **2017**, *13*, 202−209.
(183) Caricato, M.; Trucks, G. W.; Frisch, M. J.; Wiberg, K. B. Electronic Transition Energies: A Study of the Performance of a Large Range of Single Reference Density Functional and Wave Function Methods on Valence and Rydberg States Compared to Experiment. *J. Chem. Theory Comput.* **2010**, *6*, 370−383.
(184) Watson, T. J.; Lotrich, V. F.; Szalay, P. G.; Perera, A.; Bartlett, R. J. Benchmarking for Perturbative Triple-Excitations in EE-EOM-CC Methods. *J. Phys. Chem. A* **2013**, *117*, 2569−2579.
(185) Kánnár, D.; Szalay, P. G. Benchmarking Coupled Cluster Methods on Valence Singlet Excited States. *J. Chem. Theory Comput.* **2014**, *10*, 3757−3765.
(186) Dutta, A. K.; Nooijen, M.; Neese, F.; Izsák, R. Exploring the Accuracy of a Low Scaling Similarity Transformed Equation of Motion Method for Vertical Excitation Energies. *J. Chem. Theory Comput.* **2018**, *14*, 72−91.
(187) Tajti, A.; Tulipán, L.; Szalay, P. G. Accuracy of Spin-Component Scaled ADC(2) Excitation Energies and Potential Energy Surfaces. *J. Chem. Theory Comput.* **2020**, *16*, 468−474.
(188) Loos, P.-F.; Scemama, A.; Boggio-Pasqua, M.; Jacquemin, D. A Mountaineering Strategy to Excited States: Highly-Accurate Energies and Benchmarks for Exotic Molecules and Radicals. *J. Chem. Theory Comput.* **2020**, *16*, 3720−3736.
(189) Bruneval, F.; Marques, M. A. L. Benchmarking the Starting Points of the GW Approximation for Molecules. *J. Chem. Theory Comput.* **2013**, *9*, 324−329.
(190) Bruneval, F.; Hamed, S. M.; Neaton, J. B. A Systematic Benchmark of the Ab Initio Bethe-Salpeter Equation Approach for Low-Lying Optical Excitations of Small Organic Molecules. *J. Chem. Phys.* **2015**, *142*, No. 244101.
(191) Knight, J. W.; Wang, X.; Gallandi, L.; Dolgounitcheva, O.; Ren, X.; Ortiz, J. V.; Rinke, P.; Körzdörfer, T.; Marom, N. Accurate Ionization Potentials and Electron Affinities of Acceptor Molecules III: A Benchmark of GW Methods. *J. Chem. Theory Comput.* **2016**, *12*, 615−626.
(192) Caruso, F.; Dauth, M.; van Setten, M. J.; Rinke, P. Benchmark of GW Approaches for the GW100 Test Set. *J. Chem. Theory Comput.* **2016**, *12*, 5076−5087.
(193) Marie, A.; Loos, P.-F. A Similarity Renormalization Group Approach to Green's Function Methods. *J. Chem. Theory Comput.* **2023**, *19*, 3943−3957.
(194) Jacquemin, D.; Duchemin, I.; Blase, X. Benchmarking the Bethe-Salpeter Formalism on a Standard Organic Molecular Set. *J. Chem. Theory Comput.* **2015**, *11*, 3290−3304.
(195) Rangel, T.; Hamed, S. M.; Bruneval, F.; Neaton, J. B. An Assessment of Low-Lying Excitation Energies and Triplet Instabilities of Organic Molecules With an Ab Initio Bethe-Salpeter Equation Approach and the Tamm-Dancoff Approximation. *J. Chem. Phys.* **2017**, *146*, No. 194108.
(196) Hirata, S.; Head-Gordon, M. Time-Dependent Density Functional Theory within the Tamm-Dancoff Approximation. *Chem. Phys. Lett.* **1999**, *314*, 291−299.
(197) Chantzis, A.; Laurent, A. D.; Adamo, C.; Jacquemin, D. Is the Tamm-Dancoff Approximation Reliable for the Calculation of Absorption and Fluorescence Band Shapes? *J. Chem. Theory Comput.* **2013**, *9*, 4517−4525.
(198) Leng, X.; Yin, H.; Liang, D.; Ma, Y. Excitons and Davydov Splitting in Sexithiophene From First-Principles Many-Body Green's Function Theory. *J. Chem. Phys.* **2015**, *143*, No. 114501, DOI: 10.1063/1.4930975.
(199) Jacquemin, D.; Duchemin, I.; Blondel, A.; Blase, X. Benchmark of Bethe-Salpeter for Triplet Excited-States. *J. Chem. Theory Comput.* **2017**, *13*, 767−783.
(200) Grotjahn, R.; Kaupp, M. Assessment of Hybrid Functionals for Singlet and Triplet Eccitations: Why do Some Local Hybrid

Functionals Perform so well for Triplet Excitation Energies? *J. Chem. Phys.* **2021**, *155*, No. 124108.
(201) Jacquemin, D.; Perpète, E. A.; Ciofini, I.; Adamo, C. Assessment of Functionals for TD-DFT Calculations of Singlet-Triplet Transitions. *J. Chem. Theory Comput.* **2010**, *6*, 1532−1537.
(202) Goerigk, L.; Grimme, S. Calculation of Electronic Circular Dichroism Spectra with Time-Dependent Double-Hybrid Density Functional Theory. *J. Phys. Chem. A* **2009**, *113*, 767−776.
(203) Isegawa, M.; Peverati, R.; Truhlar, D. G. Performance of Recent And High-Performance Approximate Density Functionals for Time-Dependent Density Functional Theory Calculations of Valence and Rydberg Electronic Transition Energies. *J. Chem. Phys.* **2012**, *137*, No. 244104.
(204) Leang, S. S.; Zahariev, F.; Gordon, M. S. Benchmarking the Performance of Time-Dependent Density Functional Methods. *J. Chem. Phys.* **2012**, *136*, No. 104101.
(205) Holzer, C.; Klopper, W. A Hybrid Bethe-Salpeter/Time-Dependent Density-Functional-Theory Approach for Excitation Energies. *J. Chem. Phys.* **2018**, *149*, No. 101101.
(206) Avagliano, D.; Skreta, M.; Arellano-Rubach, S.; Aspuru-Guzik, A. DELFI: a Computer Oracle for Recommending Density Functionals for Excited States Calculations. *Chem. Sci.* **2024**, *15*, 4489−4503.

https://doi.org/10.1021/acs.jctc.4c00906
J. Chem. Theory Comput. 2024, 20, 8152−8174